

AD-A100 068

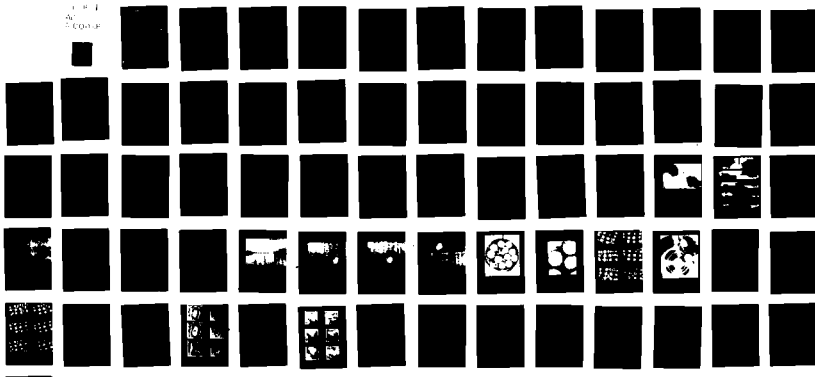
BRISTOL UNIV (ENGLAND) H H WILLS PHYSICS LAB
THE PHYSICAL MECHANISMS RESPONSIBLE FOR THE WEATHERING OF EPOXY--ETC(U)
OCT 80 J CANDLIN, B CUNNINGHAM, J P SARGENT DA-ERO-78-G-117

F/G 11/9

NL

UNCLASSIFIED

AC 1
AC 2
DODGE



END
DATE
FILED
7-8-
DTIC

ADA100068

LEVEL
12

SC AD

THE PHYSICAL MECHANISMS RESPONSIBLE FOR THE WEATHERING
OF EPOXY RESINS AND GLASS FIBRE REINFORCED EPOXY RESINS

PC-6545

Annual Technical Report

by

J Candlin
B Cunningham
J P Sargent
M D Vaudin
T W Turner
K H G Ashbee



October 1980

EUROPEAN RESEARCH OFFICE
United States Army
London England

GRANT NUMBER DA-ERO-78-G-117

H H Wills Physics Laboratory
University of Bristol

DTIC FILE COPY

Approved for Public Release: distribution unlimited

81611128

REPORT DOCUMENTATION PAGE		READ INSTRUCTIONS BEFORE COMPLETING FORM	
1. REPORT NUMBER		2. GOVT ACCESSION NO.	
		AD-A100068	
4. TITLE (and Subtitle)		5. TYPE OF REPORT & PERIOD COVERED	
The Physical Mechanisms Responsible for the Weathering of Epoxy Resins and Glass Fibre Reinforced Epoxy Resins.		9 Annual Technical Report Oct 78-Oct 80	
7. AUTHOR(s)		6. PERFORMING ORG. REPORT NUMBER	
J. Candlin, B. Cunningham, J. P. Sargent, M. D. Vauding, T. W. Turner & K.H.G. Ashbee		DAER078-G-117	
9. PERFORMING ORGANIZATION NAME AND ADDRESS		10. PROGRAM ELEMENT, PROJECT, TASK AREA & WORK UNIT NUMBERS	
University of Bristol H.H. Wills Physics Lab, Royal Fort, Tyndall Avenue, Bristol BS8 1TL		6.11.02A 16 IT161102BH57-04	
11. CONTROLLING OFFICE NAME AND ADDRESS		12. REPORT DATE	
USARDG-UK Box 65 FPO NY 09510		11 Oct 80	
14. MONITORING AGENCY NAME & ADDRESS (if different from Controlling Office)		13. NUMBER OF PAGES	
15 DA-E 0-78-6-447		60	
16. DISTRIBUTION STATEMENT (of this Report)		15a. DECLASSIFICATION/DOWNGRADING SCHEDULE	
Approved for Public Release - Distribution Unlimited			
17. DISTRIBUTION STATEMENT (of the abstract entered in Block 20, if different from Report)			
18. SUPPLEMENTARY NOTES			
19. KEY WORDS (Continue on reverse side if necessary and identify by block number)			
GRP Epoxies water uptake stress field photoelasticity		interlaminar swelling interfibre swelling ultrasound	
20. ABSTRACT (Continue on reverse side if necessary and identify by block number)			
20. The application and development of a number of optical techniques designed to obtain experimental measurements of the internal stress fields present in the matrix phase of epoxy resin based composites is described. The stress fields arise from curing and during the swelling that accompanies water uptake.			
One experiment enables the radial and tangential components of the stress			

20. A field present around an individual fibre to be measured using an oblique incidence photoelastic method. Another, particularising interlaminar swelling, uses thin plate elasticity theory to calculate stresses from the deformation of a microscope cover slip bonded to a unidirectional composite which is immersed in water at room temperature. The third exploits the photoelasticity present in and around short fibres allowing direct comparison of the loss of load transfer between commercially drawn fibres with laboratory grades of different glass fibres exposed to warm water.

Computer models have been developed which are capable of accepting the data to give a realistic analysis of states of internal stress anticipated to occur during service. Stress analysis using polarized light has been simplified by representing the changing state of polarization by the Poincare sphere construction. A finite element approach, employed for modelling the stress field normal to the fibre, treats the fibre as purely elastic and the resin matrix as elastoplastic.

A

Accession For	
NTIS GRA&I	<input checked="" type="checkbox"/>
DTIC TAB	<input type="checkbox"/>
Unannounced	<input type="checkbox"/>
Justification	
Ref:	
Distribution/	
Availability Codes	
Avail and/or	
Print	Special
A	

UNCLASSIFIED

TABLE OF CONTENTS

Section	Page	
LIST OF FIGURES		
1.	INTRODUCTION	1
2.	DEBONDING OF FIBRES IN AN EPOXY RESIN MATRIX	2
	2.1 POINCARE	2
	2.2 DISCUSSION OF THE EXPERIMENTS	6
	2.3 SUMMARY OF RESULTS	10
	2.4 DISCUSSION OF THE RESULTS	11
3.	ULTRASONIC PHOTOELASTICITY	14
	3.1 QUARTZ OSCILLATOR	14
	3.2 COMPUTER MODEL	15
4.	STRESS FIELDS	16
	4.1 CURING STRESSES	16
	4.2 INTERLAMINAR SWELLING	20
	4.3 INTERFIBRE SWELLING	22
	4.4 FINITE ELEMENTS	23
5.	CONCLUSIONS	26
REFERENCES		

LIST OF FIGURES

No.

Figure 1 Projection of the E vector helix.

Figure 2 Poincaré sphere construction.

Figure 3 Effect of a retarder on elliptically polarized light.

Figure 4 Typical experimental arrangement.

Figure 5 Poincaré sphere analysis of the above.

Figure 6 Stress induced birefringence in and around an 'S' glass fibre drawn in ammonia.

Figure 7 Series of photographs showing buildup of shear stress.

Figure 8 Schematic diagram showing the stresses in fibre and resin.

Figure 9 Isoclinics in and around a fibre misaligned with the resin background birefringence.

Figure 10 Retardation in resin vs. radial distance from fibre centre.

Figure 11 Load transfer index - E glass - 100°C - 16 mins.

Figure 12 Load transfer index vs. immersion time for four glasses cast in MY 750 resin.

Figure 13 Photograph of an 'S' glass fibre drawn in ammonia, after 6400 minutes immersion in water at 60°C.

Figure 14 Photograph of an 'E' glass fibre drawn in CF₄, after 10200 minutes immersion in water at 60°C.

Figure 15 Photograph of a commercial 'S' glass fibre after 10200 minutes immersion in water at 60°C.

Figure 16 Photograph of a commercial 'E' glass fibre after 10200 minutes immersion in water at 60°C.

Figure 17 Photograph of a transverse section of a model unidirectional composite examined with the polarising microscope.

Figure 18 Photograph of a small region of a transverse section examined with polariser and analyser crossed.

Figure 19 Photograph of transverse sections examined in both plane and circularly polarised light.
The fibres are arranged in a periodic array.

Figure 20 Photograph of a small region of a transverse section examined with polariser and analyser crossed.

Figure 21 Plot of the hoop tensile stress against radial distance from the fibre.

Figure 22 Schematic diagram showing the cracking of the glass tube in which the specimen was cast.
After immersion in water at 80°C for 4 days.

Figure 23 Photograph of transverse sections examined in plane and circularly polarised light.
After immersion in water at 80°C for 4 days.
The fibres are arranged in a periodic array.

Figure 24 Shape changes anticipated for the fillet of resin between three closely packed fibres.

Figure 25 Photograph of a single laminate (glass fibre/epoxy resin) to which is bonded a microscope cover slip.

Figure 26 Sequence of Moiré patterns for the specimen shown in Figure 25 immersed in water at 60°C.

Figure 27 Displacements and the 4th partial differentials vs. distance. The 4th partial differential shows the normal stress distribution.

Figure 28 Moiré patterns for MY 750 resin immersed in water at 60°C showing the ingress of swelling during water uptake.

Figure 29 Migration distance of the 1st Moiré fringe shown in Figure 28, plotted against the square root of time.

Figure 30 22-element mesh

Figure 31 236-element mesh

Figure 32 1% Biaxial tensile strain, small fibre,
low plasticity interface.

Figure 33 1% Biaxial tensile strain, small fibre,
high plasticity interface.

Figure 34 1% Biaxial tensile strain, large fibre,
low plasticity interface.

Figure 35 1% Biaxial tensile strain, large fibre,
medium plasticity interface.

Figure 36 1% Pure shear strain, small fibre,
low plasticity interface.

Figure 37 1% Pure shear strain, small fibre,
high plasticity interface.

1.

INTRODUCTION

Physical phenomena and mechanisms central to the degradation of epoxy resins and epoxy resin composites have been extensively examined over the two years of this Grant. The experimental and theoretical methods used have led to the identification of factors that need to be considered when substituting composites for metals as primary structural members. The programme began with attention directed towards the prevention and prediction of loss of mechanical strength, specific attention being paid to the further development and application of optical methods for monitoring loss of ability to transfer shear stress at interfaces between fibre and matrix materials. As the study has progressed, it has become increasingly apparent that direct optical methods offer reliable means for assessment of the importance of changes occurring at, or very close to, the interface.

One technique which shows considerable promise is that in which the load transferred from resin to fibre is measured photoelastically. A microscope with rectified optics has improved our facility for making these measurements and, by paying careful attention to specimen preparation, recent results have permitted comparisons to be made between fibres of different composition and different surface condition. The method used here is the only direct way that such comparisons can be made, and further development of the technique to enable the experiment to be controlled by means of a microcomputer could pay enormous dividends.

Ultrasonic photoelasticity investigations have continued in an attempt to acquire more precise data from property changes attributable to water uptake. By the very nature of its modes of propagation, ultrasound samples a very much larger region of material than that which can be sensibly identified as "the interface" and, for this reason, the technique is more sensitive to macroscopic changes such as matrix plasticisation than it is to localised changes such as the destruction of bonds at fibre/matrix interfaces. Efforts to raise the frequency and sharpen the ultrasonic fringe system are unlikely to contribute to the interfacial dialogue.

Work in this area is very relevant to non-destructive evaluation (NDE) of composites in the field. In respect of this, analysis of data collected from several transducers giving piezoelectric output, present challenging problems in both acquisition and analysis. Stress fields arising from differential contraction between fibre and resin materials and modifications of these stress fields that result from resin swelling during water uptake are now analysed by finite element method. The finite element method (fem) due to Adams and co-workers (1970) treats the purely elastic fibre and elastoplastic matrix in generalized plane strain and

provides for a pseudo-three-dimensional stress analysis. The method adopted here is that developed by Alexander and Turner (1975) for axisymmetrical flow and has been modified in order to accommodate plane strain. The interface is represented by a third phase. The analysis so far attempted parallels the methods reported by Adams.

Two new optical methods have been explored in order to secure experimental measurement of internal stresses associated with inhomogeneous resin shrinkage and swelling. The first is an oblique incidence polarising microscope method which has been used to uniquely determine the principal stresses transverse to the fibre direction in an as-cured uniaxial composite. The second method exploits the optical interference pattern created between a resin layer (actually, between a thin microscope cover slip in contact with the resin layer) and an optical flat in order to measure the resin swelling. Using thin plate elasticity theory, the resin displacements so measured have been converted to stresses.

Large scale programs have been run on the GEC 40/85 minicomputer and smaller programs, one of which receives data typed directly into an on-line computer console, use the Cromemco System 3 micro. The latter computer, now situated in our composites laboratory, is proving invaluable. Plans for the interfacing of the micro with the piezoelectric transducer for sampling a wave-form very rapidly (~16 MHz) are at an advanced stage.

2. DEBONDING OF FIBRES IN AN EPOXY RESIN MATRIX

2.1 POINCARÉ

The stresses generated in a glass fibre-epoxy resin composite during resin cure and during subsequent cooling to room temperature are small in magnitude and complex in distribution. Their analysis using polarized light is simplified by representing the state of polarization, and the change in this state as the light passes through the optical system, by means of the Poincaré sphere construction, Poincaré(1892). A single point on the surface of a sphere represents the polarization of electromagnetic oscillation at any point in the system. The changes in this polarization are represented by the motion of the representative point about the surface of the sphere in accordance with simple rules. In a polarized light wave the end point of the electric vector \underline{E} describes an elliptical helix. This helix projects on to a plane parallel to the wave-front as an ellipse whose eccentricity is described by the angle $\beta = \tan^{-1} (b/a)$, where a and b are the major and minor axes. The orientation of the ellipse with respect to some arbitrary Cartesian basis (i, j) normal to the optic

axis is specified by the angle α (Figure 1). The point P representing the state of polarization described by the angles α and β is plotted on the surface of a unit sphere at a latitude of 2β relative to the equator and a longitude of 2α relative to some arbitrary meridian (Figure 2). Conventionally, points in the upper hemisphere represent electromagnetic radiation in which the \underline{E} vector rotates anti-clockwise, and those in the lower, clockwise.

This mode of representation has several consequences that are immediately obvious. All points lying on the equator represent linearly polarized light; the two poles (North and South) represent circularly polarized light rotating anti-clockwise and clockwise respectively; points on the same parallel ($\beta = \text{constant}$) represent ellipses of the same ellipticity and different orientations and conversely points on the same meridian ($\alpha = \text{constant}$) represent ellipses of varying form but the same orientation; two points at the opposite ends of the same diameter represent elliptical helices of opposite handedness - both ellipses have the same form but the major axis of one ellipse coincides with the minor of the other.

This last proposition has an important special case when the points lie on the equator, and therefore represent two waves linearly polarized at right angles. These waves can generate any elliptically polarized wave and the Poincaré sphere can be used to determine the required phase and amplitude relationships between them. In Figure 2, I and J represent the two linearly polarized waves and P represents the elliptically polarized wave to be generated. Conversely, P represents a polarized wave, ellipticity angle β , which is to be resolved into two orthogonal linearly polarized components in the directions \underline{i} and \underline{j} , α clockwise and $90-\alpha$ anti-clockwise from the major axis (Figure 1). In both cases the construction is the same.

The \underline{E} vector of an elliptically polarised e-m wave as a function of time is

$$\underline{E}(t) = a \cos \omega t \underline{x} + b \sin \omega t \underline{y} \quad (1)$$

where \underline{x} and \underline{y} are unit vectors parallel to the major and minor axes whose lengths are a and b respectively (See Figure 1). Using axes \underline{i} and \underline{j} inclined at α to \underline{x} and \underline{y} , \underline{E} can be expressed

$$\underline{E}(t) = A \cos (\omega t - \theta_1) \underline{i} + B \cos (\omega t - \theta_2) \underline{j} \quad (2)$$

where θ_1 and θ_2 are the phase angles and A and B the amplitudes of the two waves. To compare these two expressions we express

$$\underline{x} = \cos \alpha \underline{i} + \sin \alpha \underline{j} \quad (3)$$

$$\underline{y} = -\sin \alpha \underline{i} + \cos \alpha \underline{j}$$

Substituting (3) into (1)

$$\begin{aligned} \underline{x} &= [a \cos \omega t \cos \alpha - b \sin \omega t \sin \alpha] \underline{i} \\ &\quad + [a \cos \omega t \sin \alpha + b \sin \omega t \cos \alpha] \underline{j} \end{aligned} \quad (4)$$

Expanding (2) and comparing terms with equation (4) yields

$$\begin{aligned} a \cos \alpha &= A \cos \theta_1 & b \sin \alpha &= -A \sin \theta_1 \\ a \sin \alpha &= B \cos \theta_2 & b \cos \alpha &= B \sin \theta_2 \end{aligned} \quad (5)$$

By eliminating θ_1 and θ_2 the following equations are easily obtained

$$\begin{aligned} A^2 + B^2 &= a^2 + b^2 \\ A^2 - B^2 &= (a^2 - b^2) \cos 2\alpha \end{aligned} \quad (6)$$

Putting $B/A = \tan \phi$ these two equations can be reduced to

$$\cos 2\phi = \cos 2\beta \cos 2\alpha$$

In the spherical triangle IPQ

$$\cos \hat{IOP} = \cos 2\beta \cos 2\alpha$$

hence $2\phi = \hat{IOP}$ which determines the relative amplitudes of the two waves.

From equations (5) and (6) can be obtained

$$\frac{2ab}{a^2 + b^2} = \frac{2AB}{A^2 + B^2} \sin(\theta_2 - \theta_1) \quad (a^2 - b^2) \tan \alpha = \frac{2AB}{A^2 - B^2} \cos(\theta_2 - \theta_1)$$

which on rearranging, become

$$\sin 2\beta = \sin 2\phi \sin (\theta_2 - \theta_1) \quad \tan 2\alpha = \tan 2\phi \cos (\theta_2 - \theta_1)$$

In the spherical triangle IPQ

$$\sin 2\theta = \sin 2\psi \sin \theta$$

$$\tan 2\alpha = \tan 2\psi \cos \theta$$

where θ is the angle between the equatorial plane and the plane containing I, J and P.

Hence $\theta = \theta_2 - \theta_1$, indicating that the wave represented by J lags by θ behind the wave I.

On entering a birefringent crystal, polarized light can be considered as split into two components, parallel to the fast and slow axes of the crystal in the plane normal to the optic axis. Their phase and amplitude relationships are given by the angles θ and ψ described in the previous paragraph. As the two waves pass through the crystal at different speeds their relative amplitudes remain the same but the phase difference between them changes by an angle ($\delta\theta$) proportional to the thickness (e) of crystal traversed and also to the difference in the refractive index of the crystal for light waves polarized in the fast and slow directions (Δn). In the Poincaré sphere representation, ψ remains constant and θ changes by $\delta\theta = 2\pi\Delta ne/\lambda$ radians. Assuming I and J to be the fast and slow directions respectively (Figure 3), the position of P, which represents the incident light, is rotated by $\delta\theta$ anti-clockwise about the axis IJ as indicated.

The Brace-Kohler compensator is used to measure small optical retardations, particularly in connection with photo-elastic experiments. It consists of a slice of birefringent crystal which introduces a known retardation R_o between light waves polarized in the fast and slow directions of the crystal. It is usually calibrated for a given wavelength of light and the retardation is normally quoted in nanometres of path difference. A typical experimental arrangement of crossed polars, compensator and specimen is shown in Figure 4. Initially the compensator is aligned with its fast and slow axes parallel to the axes of the crossed polars and the fast axis of the specimen is set at 45° to the polars. The compensator is then rotated through an angle ψ until the intensity of light passing through the whole system is a minimum; the retardation R due to the specimen is then given by the following expression:

$$R \approx R_o \sin 2\psi$$

The Poincaré sphere analysis of the above optical system is shown in Figure 5. P and A represent the directions of the polarizer and analyser respectively. As discussed in the previous section, the point P denoting light emerging from the polarizer is rotated by the compensator by an angle θ equal to $2\pi R_o/\lambda$ about an axis CC' lying in the equatorial plane at

an angle 2ϕ to the line PA; hence P moves to P'. The specimen rotates the point P' through an angle β equal to $2\pi R/\lambda$ about the axis SS' (perpendicular to AP) to a point P'' such that $\hat{P}O\hat{P}''$ is a minimum, the condition for minimum light intensity transmitted through the analyser. Hence P'' must lie on the equatorial circle. If we assume that $OP = 1$, then it is easily shown that

$$\cot \theta \sin \beta = \cos \theta \sin 2\phi$$

from which we obtain

$$\sin \beta = \sin \theta \sin 2\phi$$

For small retardations, the following approximation

$$R \sim R_0 \sin 2\phi$$

holds, as before.

2.2

DISCUSSION OF THE EXPERIMENTS

When an epoxy resin cures, and as it cools from the cure temperature, it shrinks and generates stresses in and around inclusions such as totally embedded short fibres. The stress fields are cylindrically symmetric with radial compressive stresses in the resin transmitted normally across the fibre/resin interface. The resin adjacent to the fibre also experiences hoop tensile stresses and a tensile stress parallel to the fibre which is under axial and radial compression. Figure 6 shows the pattern of stress-induced birefringence in and around an 'S' glass fibre drawn in ammonia and totally embedded in a slab of Ciba Geigy MY 750 epoxy resin; the fibre axis is aligned parallel to one of the crossed polars. The stress within the fibre includes a component which arises from shear stress transferred at the interface and which builds up with distance from each fibre end. The existence of axial shear stresses in the resin adjacent to the fibre ends is demonstrated by the lobes of light extending a third of the length of the fibre from both ends. The series of photographs in figure 7 taken between crossed polars at different specimen orientations (in steps of 5°) gives an indication of how the purely tensile stresses in the resin parallel to the fibre at its centre gradually acquire a shear component towards the fibre ends. The load transfer index is a measure of the build up of compressive stresses in the fibre due to interfacial shear stresses. It is expected that as the interfacial bonds break down the compressive stress build up will be reduced until, when total debonding has occurred, there will be no variation in fibre compression along its length. Figure 8 is a schematic representation of the stresses in the fibre and resin.

The load transfer index (LTI) for a given fibre is defined as the difference between the corrected retardations measured in the middle of the fibre and the average of the corrected retardations measured one fibre diameter in from both ends. The corrected retardation is the difference between the retardation measured through the fibre and the average of the retardations measured adjacent to, and one fibre diameter from, the fibre. All compensation measurements are taken with the fibre at 45° to the crossed polar axes in accordance with the procedure for measuring retardations using the Brace-Köhler compensator described in the discussion of the Poincaré sphere. During the last nine months a re-appraisal of the measurement of the LTI from a theoretical and experimental standpoint has led to a fuller appreciation of the wealth of information that can be obtained from retardation measurements through and adjacent to embedded fibres. Since a number of unquantifiable factors affect the absolute values of retardation and load transfer index, the major importance of the LTI lies in its variation and gradual decline after successive periods of immersion in warm water. However the Poincaré sphere construction has increased our understanding of the significance of the individual measurements.

The specimens studied were all cast in silicon rubber moulds. A suitable quantity of glass fibre was cut into 1-2 mm lengths, washed in acetone, dried in an oven and added to the liquid epoxy resin prior to vigorous mixing and subsequent de-gassing under vacuum. The moulds were carefully cleaned and dried, and warmed to approximately 50°C to aid in filling the mould to the desired level with the viscous resin. After gelling for 2 hours at 100°C the oven temperature was raised slowly to 150°C and the specimens were cured for a further 4 hours before slow cooling in the oven. Despite these precautions, all the specimens possessed intrinsic birefringence with the fast axis approximately parallel to the long axis contraction between resin and mould. The magnitude of this background birefringence was at least double the greatest stress-induced birefringence arising from the resin shrinking onto a fibre, hence the resultant pattern of isoclinics on and around a fibre only demonstrated the expected cylindrical symmetry when the fibre was approximately aligned with the fast or slow axes of the background birefringence. When this condition obtained the fast axes in the resins either side of the fibre end were misoriented from the fibre axis by approximately equal but opposite angles.

Using the Poincaré sphere construction it can easily be shown that if the slow and fast axes of the area of specimen being studied are not at 45° to the crossed polars, the angle of compensation is reduced. However, if the misorientation angles, although of opposite sign, are equal in magnitude (as described above), the corrections to the compensation readings are the

same. This was confirmed by the following measurements taken from a commercial 'E' glass fibre aligned at 6° to the specimen axis, at which orientation the retardations wither side of a fibre end were 19.5 nm and 17.0 nm respectively. Rotating the specimen 19.3° clockwise brought the first area into correct alignment and a reading of 25 nm was recorded. A rotation of 21.2° anti-clockwise changed the second retardation reading to 23.25 nm, hence the two readings were changed approximately in proportion. It is interesting to note that if the inverse cosines of the two ratios between uncorrected and corrected retardations are taken, the results are 38.7° and 43° respectively which are twice the misalignment angles, as predicted by the Poincaré sphere construction.

Photographed between crossed-polars, the fibre in Figure 9 was surrounded by a symmetrical pattern of isoclinics similar to Figure 6 but the fibre itself was not completely dark. Rotating the specimen 4° clockwise rendered the fibre dark but destroyed the cylindrical symmetry of the resin pattern. This is an example of slight misalignment between the stress-induced and background birefringence. In more extreme cases, it was not possible to orient the fibre so that the isoclinics displayed cylindrical symmetry. The isoclinics were always zero order but because of the background birefringence they did not necessarily indicate regions of the specimen in which the principal stress directions were aligned with the crossed polars.

The fibres studied were of four types - commercial 'E' and 'S' glass, 'S' glass drawn in a dry ammonia atmosphere and 'E' glass drawn in a tetrafluoromethane (CF_4) atmosphere (these two laboratory glasses were supplied by David Martin); in the main experiment two of each type of fibre were studied. The commercial fibres were all 10 microns in diameter but for the laboratory fibres the 'E' glass fibres were 6 microns and the 'S' were 13 microns. Each measurement of LTI entailed a minimum of nine compensation readings, three at each end and three in the middle of the fibre. A corrected retardation was also obtained approximately midway between the middle and one end. In addition the background compensation in the resin away from the influence of any fibre induced stresses was recorded together with the "balance" compensation at which the intensity of light passing through the fibre centre was the same as that passing through adjacent resin.

All the retardations are theoretically calculable as integrals along the light path and correspond to more or less complex curves on the Poincaré sphere. The retardation of light passing through the fibre has components due to the differences between (i) the hoop and axial stresses (both tensile) in the resin, and (ii) the radial and axial compressive stresses in the fibre. Retardation in the resin next to the fibre centre is a relatively simple case as the axial tension and the resultant of hoop and

radial stresses are always aligned with the crossed polars. At the fibre ends, the situation is complicated by the shear stresses in the resin which result in the principal stress directions being misaligned with the fibre, as discussed above. The magnitudes of these various stresses are determined initially by the fibre geometry, the difference in thermal expansion coefficients between resin and glass and the position of the fibre within the slab of epoxy resin (the fibres tend to settle between 5 and 20 microns from the bottom of the specimen). By symmetry the interfacial shear stress at the centre of the fibre is zero. Mismatch between fibre and resin as a result of resin shrinkage increases with distance from the fibre centre, x , producing shear stresses which, according to Cox (1952), are proportional to $\sinh(x)$. The radial compressive and hoop tensile stresses are, according to simple theories, equal in magnitude and both fall off as $1/r$ where r is the radial distance from the fibre axis. Their magnitudes were expected to depend on fibre thickness, being greatest for the 13 micron laboratory 'S' glass fibres and least for the 6 micron laboratory 'E' glass. This was borne out by experimental observation in that the retardation in the resin next to the fibre centre differed from the background retardation by 11.5 nm for a laboratory 'S' glass fibre, 5.85 nm for commercial 'S' glass and 1.5 nm for laboratory 'E' glass. The variation of retardation with radial distance from the axes of the laboratory 'S' glass fibre is shown in Figure 10 and shows the expected $1/r$ dependence.

The proximity of the fibres to the specimen surface allows stress relaxation at the surface to occur reducing the magnitude of the stresses generated. It is noticeable, when considering the raw data that the thinner the fibre, the greater the variation in retardation along the length of the fibre and the less the variation of the retardation in the resin. This indicates a greater stress variation in the thinner fibres due to its smaller cross-sectional area. In addition it is known that exposing the epoxy resin to water alters its stress optic coefficient and causes swelling. Work is in progress to investigate these phenomena. At this stage some idea of the magnitude of these effects can be gleaned from the variation in background birefringence which changed by a maximum of 5.85 nm for any one specimen during the complete run and the typical change was of the order of 1 nm between immersions. 1 nm of retardation in polarised light passing through 50 microns of epoxy resin indicates a principal stress difference of $3.5 \times 10^5 \text{ N/m}^2$ assuming a stress optic coefficient of 56 Brewsters.

2.3

SUMMARY OF RESULTS

A decision was taken early in the second year of work to carry out the water immersion tests at 60°C. It was found that if the specimens were boiled, the debonding process occurred in a catastrophic fashion with little significant variation of load transfer index before the sudden and total loss of interface integrity. As an example of this behaviour, the SYMVU plot (Figure 11) of corrected retardation at various positions along an 'E' glass fibre drawn in CF₄ against immersion time in boiling water shows that after 15 minutes the fibre 'lost contact' with the resin and there was as a result no variation of stress along the length of the fibre. A similar test on commercial 'E' glass indicated total loss of load transfer after 13 minutes, an insignificant variation considering the individual immersions were of longer duration. It was expected that at 60°C the processes of deterioration would progress fast enough to be observable over a realistic time span. In the light of data collected since that decision, it is appropriate for further work to be carried out at 75°C. Above 80°C the diffusion coefficient of water in MY 750 departs from the normal Boltzmann variation with temperature. At 60°C an overnight soaking frequently produced little or no effect on the fibres.

Figure 12 summarises the data obtained from the specimens during 170 hours of immersion in water at 60°C. The large variations in load transfer index which occurred in all cases during the first 1500 minutes is not wholly attributable to experimental error which was ± 2 nm in the LTI. The general downward trend of each graph is overlaid with fluctuations which arise from the change in stress optic coefficient and resin swelling as described above. The thinner glass fibres ('E' in CF₄) appeared to have less load transferred to them and the 'S' glass in ammonia fibres initially had higher values of LTI than the commercial fibres. However during immersion, several bubbles developed on the surface of the two 'S'-in-ammonia fibres, indicating total debonding particularly at the fibre ends. Figure 13 is an optical micrograph of one of these fibres after 6400 minutes immersion. The load transfer index reflected this deterioration, falling to 3.4 nm for the fibre in figure 13 and 1.1 nm for the other. The other fibres all experienced the initial slight drop in LTI but during the final 80% of the immersion time there was no significant change. because time was running short the specimens were placed in boiling water for 1 minute and then left in the water as it slowly cooled. The effect on this treatment was in some cases considerable as can be seen from the micrographs in figures 14, 15 and 16. In particular the 'E' glass fibre drawn in CF₄ (figure 14) debonded almost completely towards the ends. The commercial 'S' glass fibres were least affected by the boiling treatment. The bubble visible at the end of the fibre in Figure 15 existed prior to boiling which served to increase its size. It seems likely that the boiling caused small invisible bubbles of

water to form in regions of high water content and coalesce into the large visible bubbles seen in the micrographs. The test pointed up the unsuitability of boiling as the normal test mode. The commercial 'E' glass fibre in figure 16 was more affected than commercial 'S' glass, with the level of debonding rising to about 50% at the fibre end. It was noticeable that the bubbles formed preferentially in the regions of highest shear stress at the ends of the fibres. This may have been a factor in the rapid debonding of the 'S' glass drawn in ammonia since experiments showed that these fibres had the highest levels of interfacial shear stress.

The results of the initial tests carried out during the first year of work are summarised in Table 1. These were in the nature of exploratory tests and indicate the need for the more sophisticated approach adopted in the second year.

2.4

DISCUSSION OF THE RESULTS

The research has shown that the load transfer experiment is a useful and necessary simplification of a complex physical process. The subtraction of the retardation in resin adjacent to the fibre does not afford a perfect correction to the retardation through both resin and fibre but results have shown that the load transfer index measured in this way provides a simple way of assessing the load bearing capabilities of the fibre resin interface. Points germane to the experimental technique are discussed below, and this is followed by a critical evaluation of the results, emphasising their relevance to assessing the suitability of various fibre chemistries for reinforcing epoxy resins.

It was found vital that all fibres studied underwent the same regime of preparation and immersion. In practice it was a simple matter to place all the specimens in the same water bath thus fulfilling the second criteria. However, the preparation of the specimens posed more logistical problems since, from a batch of six epoxy resin specimens containing short fibres, there were on average only one or two fibres per specimen worthy of study. In section 2.3 some of the factors that might influence the value of the LTI, when no changes in the properties of the interface had occurred, were discussed. These included variation in the resin stress optical coefficient with water content, the stresses produced by inhomogeneous resin swelling due to water ingress and the position of the fibre relative to the surface of the specimen. Rotating the mould in the oven during gel would create a more random distribution of the fibres in the specimen but would also lead to problems due to resin flow before and during gel, and also due to fibres lying at an angle to the specimen surface. This would complicate the interpretation of the measured

RESIN	FIBRE	WATER TEMPERATURE	TIME TAKEN TO DEBOND
MY 750	Carbon 'A'	22°C	no debonding in 81 days
	Carbon 'A'	100°C	~ 9 hours
	Carbon 'H'	22°C	no debonding in 81 days
	Carbon 'H'	100°C	~ 15 minutes
	'E' glass (NH_3 drawn)	22°C	40-53 days
	'E' glass (NH_3 drawn) coupled*	22°C	40-53 days
	'E' glass (NH_3 drawn) coupled*	100°C	< 1 1/2 hours
	'E' glass (NH_3 drawn) coupled*	100°C	~ 1 3/4 hours
	'S' glass (NH_3 drawn)	22°C	36-49 days
	'S' glass (NH_3 drawn) coupled*	22°C	36-49 days
	'S' glass (NH_3 drawn)	100°C	22 hours
	'S' glass (NH_3 drawn) coupled*	100°C	22 hours
SP 250	S2 glass	22°C	25 days
	S2 glass	80°C	1-5 days
MY 720	'S' glass (NH_3 drawn)	22°C	9 days
	'E' glass (NH_3 drawn)	22°C	9 days
	456 (S2) glass	22°C	8 days
	P263A (S2) glass	22°C	8 days
	801 (E) glass	22°C	not debonded in 8 days
	H + S 904 (S1) glass	22°C	not debonded in 8 days
	S glass (NH_3 drawn)	80°C	< 20 1/2 hours
	456 (S2) glass	80°C	1-2 hours
	P263A (S2) glass	80°C	1 hour
	801 (E) glass	80°C	1-2 hours
	H + S 904 (S1) glass	80°C	1-4 days

* Fibres coated with silane coupling agent, A187, manufactured by Union Carbide

TABLE 1. Loss of load transfer by various composite specimens during exposure to water

retardations. The ideal specimen would contain fibres of the same uniform shape and size embedded at equal distances from the surface in otherwise stress-free resin. However, knowledge of the changes induced by departures from this ideal, together with informed observation of the visible effects of water attack, allow realistic comparisons to be made.

The 'S' glass fibres drawn in the laboratory contain, or are coated with, water soluble constituents, dissolution of which material creates pressure pockets at the fibre/matrix interface after 170 hours of exposure of the composites to 60⁰C water. The fact that premature failure is not observed with laboratory drawn 'E' glass fibres (i.e. failure which is premature compared with the behaviour of commercially drawn 'E' glass fibres) is attributed to the differences in chemical nature of the gaseous atmosphere into which drawing takes place. It is understood that Professor Martin used a tetrafluoromethane (CF₄) atmosphere for his 'E' glass fibres and an ammonia (NH₄) atmosphere for his 'S' glass fibres. Ammonium salts are readily soluble in water, saturated aqueous solutions of which generate osmotic pressures having magnitudes in excess of 100 bars at the boiling point and probably also at 60⁰C. The adhesive strength of glass/wet epoxy resin joints at 60⁰C is expected to be of the same order of magnitude.

3.

ULTRASONIC PHOTOELASTICITY

The photoelastic method for imaging ultrasound was developed for investigating the material property changes at or near glass interfaces, Turner and Ashbee (1978). Use of a light emitting diode controlled by TTL, Andrews and Wallis (1977), gave pulse widths of 50 ns, and by measuring velocities of the longitudinal and shear waves, it is possible to observe the influences of interfacial healing, continuing cure of heated specimens, plasticisation on water uptake and debonding on weathering, Farrar, Turner, and Ashbee (1979). Such data give information about the bulk material and details of the properties of the interfacial bond are not available. Experimental difficulties encountered include

(a) rapid attenuation of the ultrasound signal and

(b) poor resolution arising from the frequency which, at 2 MHz, is somewhat low for collecting data. It was therefore decided that the interface might be more easily studied in specimens of single crystal quartz and epoxy resin. Changes in mechanical damping characteristics during water uptake should be revealed by using such resin coated quartz piezoelectric crystals to drive the transducer in visualization experiments. The large amount of data contained in photographs is not easily extracted from the wave trace and the analysis must await the computer interface which will enable the changes in damping characteristics to be analysed completely.

3.1

QUARTZ OSCILLATOR

The state of localised stress near the interfacial region that is introduced during curing precludes the direct observation of ultrasonic fringes in the resin. Successful application of the technique is restricted to observation of fringes, in an adjacent stress free visualizing block, i.e. remote from the specimen. In order to investigate SiO_2 /epoxy resin interfaces more directly, a series of experiments have been carried out where the PZT5A piezoelectric discs are replaced by crystalline quartz. X-cut slabs, 2 mm thick, were sawn from a synthetic quartz single crystal having a cross-sectional area of about 2 cm. The slabs were then polished, cleaned and coated with 1 mm of Ciba-Geigy MY750 epoxy resin. An electric field up to 800v. was applied across the epoxy/quartz/epoxy with aluminium foil electrodes, and then shorted using a thyristor. The resonant mechanical vibration, observed on an oscilloscope, begins with an amplitude of 15v. and decays in about 15 cycles. The measured frequency is typically 39 MHz which is more than an order of magnitude higher than the expected frequency of 1.44 MHz. The complexity of the signal is made up of a series of modes of vibration of the quartz together with the reflections from the epoxy coating with the major component ~1.5 MHz, expected from the thyristor voltage cut-off rate, 'lost' in the total waveform. The interfacial bonding on boiling the

specimens in distilled water modifies the frequency trace by changing the relative pulse heights. The energy emanating from the quartz slabs so far investigated is not sufficient to drive a transducer for ultrasound visualisation, but the modified trace is there for analysis. It was decided to analyse the signal by means of the computer. Sampling the form of the wave by means of a fast A/D converter is regarded as the most effective method and the technique to do this has been designed.

Work in this area was suspended pending the filing of a patent application. However, owing to unintentional public release of our final technical report under Grant DA-ER0-76-G-068 (R-D No 2160), the patent application has not been filed.

3.2

COMPUTER MODEL

The work on ultrasonic photoelasticity has contributed less to interfacial physics for one principal phenomenon: stress waves can never be observed using the visualisation techniques, Turner & Ashbee (1978), in a stress gradient. It was nevertheless quickly realised that the ultrasound could pick up useful data, in a mode converting reflection, and pass on into a stress free zone where the fringes could be observed. Experimentation with composites acoustically coupled to a visualising quartz block was found to be effective although attenuation particularly of the transverse wave is significant. Steel specimens similarly coupled exhibit less attenuation since the electron and crystal dislocation scatter in metals is smaller than that produced in two phased composites. Work on the steel specimens proceeded along NDE lines and has been reported elsewhere, Kitson, Low and Turner (1979). The computer model originally designed for composite specimens and described by Turner & Ashbee (1978), has since been applied to the non-destructive application with developments to improve the graphics on our own computer equipment with the interface between the specimen and visualising block taken into account.

4.

STRESS FIELDS

4.1

CURING STRESSES

Differential thermal contraction between fibre and matrix materials during cooling from the cure temperature is not accommodated by resin flow and the state of self-stress attributable to this source has been calculated for simple fibre geometries by Adams and co-workers (1979) & (1977). They assume that the contraction is uniformly distributed and in glass fibre/epoxy resin systems, their finite element model predicts that the radial principal stress is tensile along the line of centres between adjacent fibres and compressive elsewhere, and that its magnitude at the fibre/resin interface is in the range 100 MPa to -80 MPa.

The aim of this aspect of the present research is to measure two of the principal components of the self-stress field of a glass fibre/epoxy resin composite in the as-cured state.

In order to reduce the problem to one of two-dimensional elasticity, thin transverse sections were cut from a long unidirectional composite. Accommodation of shrinkage by way of rigid body displacements in the transverse plane were prevented by casting the composite inside a thick walled glass tube. The unrelaxed radial and hoop principal stresses within any slice subsequently removed from the specimen were then amenable to measurement by the oblique incidence photoelastic method described by Durelli and Riley (1965).

The two-dimensional stress-optic law for a beam of light that enters the surface of a thin transverse section at normal incidence is

$$R = \frac{Ct}{\lambda} (\sigma_1 - \sigma_2) \quad (7)$$

where σ_1 and σ_2 are the principal stresses in the transverse plane

λ = wavelength of the light

C = stress optical coefficient

t = thickness of transverse section

In terms of the fringe order n, equation (1) becomes

$$n = \frac{Ct}{\lambda} (\sigma_1 - \sigma_2) = \frac{2Ct}{\lambda} \tau_{\max} \quad (8)$$

τ_{\max} = maximum shear stress in the transverse plane

Equation (8) can also be written as

$$\tau_{\max} = \frac{n\lambda}{2Ct} = nF \quad (9)$$

where

$$F = \frac{\lambda}{2Ct} \quad (10)$$

is the model stress fringe value.

The model stress fringe value is the change in maximum shear stress necessary to produce a change of unity in the fringe order. The quantity

$$Ft = \frac{\lambda}{2C} = f \quad (11)$$

is independent of the thickness of the model and is called the material stress fringe value. f is the change in maximum shear stress required to produce a change of unity in fringe order in a model of unit thickness. Substituting equation (5) into equation (2),

$$n = \frac{\tau_{\max}}{f} t = \frac{(\sigma_1 - \sigma_2)}{2f} t$$

Let the specimen be rotated about principal axis 1, through an angle θ . The path length (t_o) of the light becomes

$$t_o = \frac{t}{\cos\theta} \quad (12)$$

and the principal stresses transform to

$$\sigma_1 ; \sigma_2 \cos^2\theta \quad (13)$$

Let

$$a_1 = \frac{\sigma_1 t}{2f}; \quad a_2 = \frac{\sigma_2 t}{2f}$$

The corresponding fringe orders identified by $n_o^{(1)}$ are

$$n_o^{(1)} = \frac{(\sigma_1 - \sigma_2 \cos^2\theta)t}{2fc\cos\theta} = \frac{(a_1 - a_2 \cos^2\theta)}{\cos\theta} \quad (14)$$

$$a_1 = \frac{\cos\theta(n_o^{(1)} - n \cos\theta)}{\sin^2\theta}$$

$$a_2 = \frac{n_o^{(1)} \cos\theta - n}{\sin^2\theta}$$

Therefore:

$$\sigma_1 = \frac{\cos \theta (n_o^{(1)} - n \cos \theta) 2f}{t \sin^2 \theta} \quad (15)$$

$$\sigma_2 = \frac{(n_o^{(1)} \cos \theta - n) 2f}{t \sin^2 \theta}$$

Model epoxy resin unidirectional composites containing 0.5mm diameter glass filaments have been cast inside glass tubes whose dimensions are 5mm OD and 3mm ID. Prior to casting, all the glass components were thoroughly cleaned using the following procedure:

- 1) Ion-bombardment
- 2) De-oxidation by exposing for 10-15 minutes to a mixture consisting of
 170ml HNO_3
 30ml HF
 800ml distilled water
- 3) Tap-water spraying, 10-15 minutes
- 4) Deionised water spraying, 2 minutes
- 5) Drying in hot air, minimum of 30 minutes
- 6) Cooling to room temperature, maximum of 120 minutes

Small bundles of fibres, usually about 10 or 12, were gathered together and inserted into the glass tube. In the early stages of the investigation no attention was paid to the packing arrangement, the fibres usually adopting an irregular array. Epoxy resin (Araldite MY753 manufactured by CIBA-GEIGY (UK) Ltd) was then driven into the specimen until all the air, including all visible bubbles, had been displaced. The resin was gelled at room temperature for 2 days and cured at 60°C for 6 hours in accordance with the manufacturer's recommendations.

1mm thick transverse sections were removed from the specimen at intervals along its length using a high speed diamond impregnated annular saw. In order to render the sections optically transparent and avoid corrections for refraction when examined by oblique incidence, it was necessary to coat lightly the as-cut surfaces with immersion oil.

Figure 17 is a photograph of one such section examined with a Nikon Apophot 180-00-103 polarising microscope.

Figure 18 is an enlargement of a small region taken from another section of the same specimen and shows the complexity of the stress birefringence created during cooling from the cure temperature.

The range of stress birefringence resolved in these figures is large, there being several fringe orders present. In an attempt to reduce the complexity of the stress pattern and to render it amenable to comparisons with theoretical investigations, specimens with parallel fibres arranged in a periodic array were prepared. Individual 5cm fibre lengths were carefully laid up outside of the tube in a rectangular array and their ends locked into position with quick-setting epoxy resin. The fibre bundle so obtained was then cleaned in the normal way and inserted into the glass tube with the ends outside of the tube. Epoxy resin was then driven into the tube and allowed to gel, the fibre ends were cut off and the tube cut into two equal lengths which were then placed in an oven to effect curing. Using this technique it was possible to obtain two nearly identical specimens, one of which could be retained as a control specimen.

Figure 19 shows photographs of 1mm thick transverse sections cut from various positions along a 2cm length of specimen. The fibres were arranged on a rectangular grid and photographs were taken using both plane and circularly polarised light. Although stress differences revealed by the isochromatics vary non-linearly along the length of the specimen, the general distribution of the in-plane stresses near the fibre is consistent with finite element method (f.e.m.) calculations. It is interesting to note that large stress gradients surround some fibres and fringe orders of at least 5 can be counted.

Figure 20 shows a photograph of a 1 mm thick transverse section cut from the middle of a specimen which exhibited both well defined fringes and a large retardation. The image was taken with plane polarised light incident normally upon the specimen.

Figure 21 shows a plot of the hoop stress (σ_2) vs distance from the fibre for one of the fibres seen in figure 20. The units of stress are λ/Ct . With $\lambda = 546\text{nm}$, $t = 1\text{mm}$, and using $C = 56.6 \times 10^{-12} \text{m}^2/\text{N}$, λ/Ct corresponds to a stress of 9.65 MN/m^2 . The hoop principal stress at the fibre/resin interface is therefore of the order of 100 MPa falling to approximately 20 MPa one diameter from the fibre. The radial stress is compressive and is approximately constant (6 MPa) with distance from the fibre.

A specimen having similar geometry to that reported in figure 3 was immersed in distilled water at 80°C for 4 days. On removal from the water, the glass tube in which the specimen was cast was observed to have cracked at each end, as shown schematically in figure 22. Large stresses generated during resin swelling were responsible for the cracking. The specimen was sectioned in the usual manner and examined in the polarising microscope. The stress bi-refringence patterns are shown in figure 23. Very little stress birefringence was detected at any section along the length between the cracked ends.

Whilst the general form of the birefringence patterns indicated a relatively complex stress distribution, certain fibres exhibited very little asymmetry in the stress field. The birefringence patterns observed in figure 20 shows a symmetrical stress field with clearly defined radial and hoop principal stresses. The hoop stress ($\sigma_{\theta\theta} = \sigma_1$) is very much larger than the radial stress ($\sigma_{rr} = \sigma_2$). The fact that σ_{rr} does not vary significantly with r means that the maximum shear stress, $(\sigma_{\theta\theta} - \sigma_{rr})/2$, rapidly increases near the resin/fibre interface, i.e. that molecular orientation, if it occurs, is expected to be localised adjacent to the fibre. The largest measured shear stress, 47 MPa, was at a distance of some 25 μm from the fibre/resin interface. Interpolation of the data to smaller distances suggests that the 20°C yield strength of dry resin (~ 100 MPa) would be exceeded at about 15 μm from the interface.

The resin swelling that accommodates water uptake in composite materials will depend on the concentration of diffused water and is expected to be larger near to than it is remote from regions of water access. If otherwise unconstrained, the fillet of resin between three closely packed fibres would endeavour to undergo the shape change sketched in figure 24(b). Eventually, the swelling in resin in contact with the source of water molecules would saturate and the regions of maximum swelling will move inwards as indicated in figure 24(c). In the specimens studied here, the resin was not free to adopt these shape changes. The mechanical constraint offered by the glass tube surrounding the composite specimen caused the resin swelling to generate a pressure of magnitude sufficient to burst the glass tube.

4.2

INTERLAMINAR SWELLING

One source of internal stress to be considered when discussing the problem of delamination after long in-service lifetimes is inhomogeneous swelling of interlaminar resin. Swelling of this resin arises from the ingress of water from the outside and is larger close to than it is remote from the external surface. There is an additional cause of inhomogeneity in the magnitude of interlaminar swelling, namely that due to in-plane anisotropy of the diffusion coefficient for water migration; Kaelble (ref - 2nd Annual Army Composites Research Review 1979) reports values of 0.94 to 10.40 and 0.22 to $0.75 \times 10^{-8} \text{ cm}^2 \text{ sec}^{-1}$ in interlaminar diffusion parallel and perpendicular to the fibre direction in glass fibre reinforced epoxy. (OCF52/Narmco 5205). In order to investigate the interlaminar stress field attributable to water uptake, the following experiment has been devised:

Figure 25 is a photograph of a single laminate (glass fibre/epoxy resin) to which is bonded a microscope cover slip. By placing the free surface

of the cover slip in close proximity to an optical flat, a pattern of Newton's rings is created in the air gap between the two. When the specimen/optical flat assembly is exposed to an aqueous environment, the resin bonding the cover slip to the laminate swells and progressively modifies the pattern of Newton's rings. By superimposing successive photographs of the changing pattern on to a photograph of the pattern seen at the outset, it is possible to create Moiré fringes which bear a 1:1 correlation to the swelling geometry.

Figure 26 is an example of results so obtained for an S1/epoxy laminate immersed in deionised water at 60°C. The Moiré fringes are the fringes adjacent to the edges of the square cover slip. Successive fringes are the loci of displacements normal to the cover slip that differ in magnitude by half a wave length. The displacement fields parallel and perpendicular to the fibre determined after 167 hours' exposure are summarised in figure 27.

Thin plate elasticity theory predicts that the 4th differential of the axial displacement (w) of a membrane that is rigidly supported at its rim is proportional to the pressure (p) acting across it.

$$\nabla^4 w = 0 \text{ if } p = 0 \\ \text{and } D\nabla^4 w = -p \text{ if } p \neq 0$$

the flexural rigidity

$$D = \frac{2Eh^3}{3(1 - v^2)}$$

where $2h$ = the thickness of the cover slip and v is Poisson's ratio.

Figure 27 shows a graphical representation of w measured both parallel and perpendicular to the fibre direction after 167 hours' exposure to 60°C water, and the 4th differential of w . Here the maximum stress is 3 bars tensile. This contrasts with the very much larger maximum stress of 8.00 bars tensile obtained with similar experiments on glass to glass joints (section 4.3). The maximum stress perpendicular to the fibre direction after the same time of exposure to 60°C water is 3 bars. Since the origin of the stress field generated during water uptake is the inhomogeneous nature of the associated swelling (if the water and hence the swelling was uniformly distributed, the resin would be stress-free) the fact that the stresses between the lamina in composite materials are apparently very much smaller than those measured between adherends in adhesive joints is attributed to experimental difference (Redux 312/5 instead of American Cyanamid FM1000, and 640μm instead of 150μm for the cover slip thickness) and to a more uniform distribution of the diffused water. The latter would presumably indicate a marked difference in water diffusion kinetics.

At the first Annual Army Composites Research Review (1978), Professor D Adams presented a finite element model for the stress field in a unidirectional composite that has experienced uniform differential thermal contraction between fibre and matrix materials and uniform swelling of matrix material following water uptake. The assumption of uniform swelling is not justified; the flux of diffused water received by the fillet of resin located between a bundle of closely packed fibres, is not isotropic and, even for the case of a composite that is uniformly saturated with water, the swelling is strongly inhomogeneous as indicated by the sketches shown in figure 24. Of special interest, because of its proximity to the resin/fibre interface, is the Π -shaped film of resin between two adjacent fibres. In the absence of wicking, the curved surfaces of this film are shielded from water by the presence of the fibres, i.e. water uptake is restricted to diffusion more or less parallel to these curved surfaces. To investigate the swelling inhomogeneity that accompanies this pattern of water uptake and hence calculate the inhomogeneous elastic field created if (as is nearly true in a real composite) the resin is constrained not to swell, a model specimen consisting of a microscope cover slip bonded with epoxy resin to a massive and therefore rigid block of glass, has been prepared. As described in section 4.1 for the interlaminar swelling specimen, when the free surface of the cover slip is brought into contact with an optical flat, a pattern of Newton's rings is formed in the gap trapped between them. When the shape of the gap changes, as happens when the resin absorbs water, swells and displaces the cover slip, the pattern of Newton's rings changes and superposition of photographs taken before and after the changes produces a set of Moiré fringes which faithfully reveals the geometry of the resin swelling.

Figure 28 shows a sequence of photographs for a square specimen manufactured using MY 750 epoxy resin. The cover slip was approximately $150\text{ }\mu\text{m}$ thick and the resin layer approximately $50\text{ }\mu\text{m}$ thick. All glass surfaces were thoroughly cleaned before specimen assembly. Water uptake was achieved by immersing the specimen in distilled water at 60°C . From the distribution of fringes it is evident that the swelling is strongly inhomogeneous and that it faithfully reflects the geometry of the specimen for a considerable length of time. It should be noted that a Moiré fringe having moved and been replaced by its neighbour represents an increase in thickness due to swelling of half a wavelength, i.e. a percentage increase of approximately 0.5%. (The broad fringes running across the centre of the specimen and seen towards the later stages of the test are a result of the specimen tilting relative to the optical flat. With improved temperature control and better support for the specimen, the

incidence of such fringes has been almost eliminated). In figure 29 the position of the first Moiré fringe is plotted as a function of time. Since this fringe corresponds to a relatively large water concentration its migration is relatively slow and only the early stages of its progression are recorded. For points near to the rim and midway along a specimen side, a linear relationship is expected if the resin swelling is governed by Fickian behaviour. Within the limits of experimental error, the relationship is linear.

Using the $\nabla^4 w$ analysis outlined in section 4.2, it has been calculated that the maximum stress developed in this specimen is in excess of 800 bars tensile.

4.2

FINITE ELEMENTS

The classical fem paper of Turner, Clough, Martin and Topp (1956) has been developed and extended principally by Zienkiewitz (1977) and, for application to the microscopic behaviour of fibre composites, by the University of Wyoming group. The principles of the displacement formulation of the fem for plane strain have been applied to the program using triangular elements and linear shape functions. Figure 30 shows the mesh used for developing the program. The region bounded by nodes 1, 5, 7, 9, 1 represent the fibre with the remaining mesh representing the epoxy resin matrix. Figure 31 shows a more realistic mesh with fibre bounded by 1, 19, 35, 1, where the region 19, 36, 52, 35, 19 may be treated as interfacial, again with the remainder representing the matrix. The mesh of figure 31 with 236 elements and 137 nodes is generated logically in the computer. This enables the mesh to be modified for larger fibres, for interface manipulation, and for shape changes. This last point is regarded as particularly important since in the form shown, i.e. a square, the symmetry may be too high for real composites: changing the right angle of the mesh to an arbitrary value or 60° say, is easily achieved. Both mesh dimensions are 7 microns square, corresponding to a fibre diameter of 9.3 microns and a fibre volume ratio of 39%.

The strain in an element as a function of the nodal displacements is given by the strain shape matrix $[B]_e$, the suffix e relating to a single element. The use of a linear displacement shape function leads to a $[B]_e$ independent of x and y, and a constant elemental strain. Linearity of the displacement function and the coupling of neighbouring elements at nodal points ensures continuity of displacement across element boundaries, and

compatibility conditions are automatically fulfilled.

There is a matrix $[D]_e$ which when multiplied by the strain vector, gives the stress vector derived in terms of the elastic constants. The stress system is equivalent to a set of forces acting at the nodes of the element. The force vector $\{F\}_e$ may be expressed as

$$\{F\}_e = [B]_e^T [D]_e [B]_e \{a\}_e$$

where $\{a\}_e$ is the displacement vector.

$$\text{or } \{F\}_e = [K]_e \{a\}_e$$

where $[K]_e$ is a 6×6 matrix called the elemental stiffness matrix.

Corresponding to this equation is a global stiffness equation

$$\{F\} = [K] \{a\}$$

where the two vectors represent the forces and displacements at every node in the mesh. The displacement vector is found by inversion of the stiffness matrix when the loading condition is formulated in terms of known forces, and unknown forces can be calculated from known displacements. Strains and stresses may then be calculated.

The fibre is treated as purely elastic whereas the resin matrix is considered to be stressed beyond yield and into the plastic region, i.e. resin plastic strain must be added to resin elastic strain. Thus, in the program, loads are applied in increments which follow the plastic stress-strain curve by evaluating a new stiffness matrix for each new increment. Displacements and strains are calculated for each increment as in the elastic situation. The method is known as the tangent modulus method because the stress-strain matrix is found by using, instead of Young's Modulus, the tangent to the $\sigma - \epsilon$ curve at a given strain. The von Mises yield criterion is assumed together with the Prandtl-Reuss flow rule. Initially the whole load is applied to solve for the elastic formulation and if any elements are stressed beyond the yield criterion, all quantities are reduced in proportion to bring them within the elastic regime. The program then proceeds by loading incrementally where, at the end of each increment, the incremental strains are added to the current components of strain and new equivalent stresses and strains are calculated.

The stage has been reached where the program is functioning well for elastoplastic matrix resin and elastic fibre, and the first results for

biaxial tensile strain and pure shear are shown in the figures 32-37. Figure 32 shows the final mesh shape superimposed on the initial undeformed mesh for a 1% biaxial tensile strain. The resin matrix has the properties of an epoxy resin containing a water concentration of 2% and is referred to in the legend as low 'plasticity'. The crossed lines inside each element indicate the orientation and relative magnitudes of the principal stresses, the program having been written so that the vector lengths fit inside the smallest element. Figure 33 distinguishes a third phase, in that the row of elements adjacent to the fibres have properties of an epoxy resin containing a water concentration of 6%, the remaining matrix still containing 2% water, and is referred to as a 'high plasticity' interface. Figure 34 is similar to figure 32 except that the fibre has been enlarged by including an extra row of elements in the fibre, and demonstrates the mesh flexibility. Figure 35 is similar to Figure 33 but with the enlarged fibre and with the row of elements adjacent to the fibre containing 4% moisture. Figures 36 and 37 show the consequences of a 1% extension in the x-direction combined with a 1% compression in the y-direction, i.e. the consequences of macroscopic pure shear. Compressive principal stress vectors are barred at their ends.

5.

CONCLUSIONS

1. By comparing optical retardation measurements made through parallel diameters in individual fibres in order to detect interfacial load transfer, it has been demonstrated that the behaviour of epoxy resin composites during hot water uptake is different for different fibre chemistries. Not only are there differences between 'E' glass and 'S' glass fibre composites, but also between commercial and 'contaminant free' fibres of each glass composition.
2. S2/SP250 composites, prepared with the resin components mixed in accordance with the manufacturer's recommendations for a stoichiometric mix, are not sufficiently transparent for optical retardation experiments of the kind reported in conclusion 1.
3. An S2/SP250 composite panel fabricated at AMMRC is bounded by a flash which contains a low volume fraction of short fibres and which since it is transparent, is eminently suitable for optical retardation experiments to measure times for loss of load transfer during water uptake. At 80°C fibres lying parallel to and 100 m from the external surface lose their load transfer ability after 80 hours exposure to deionised water..
4. Using photoelastic visualization of ultrasound, it is possible to provide a visual display of the effects of water uptake on ultrasound velocities in composite materials.
5. The swelling associated with water uptake by resin samples having geometries representative of regions of resin in real composites, including composite laminates, is strongly inhomogeneous. The magnitudes of the corresponding swelling stresses (10's of bars) are of the same order as those due to differential contraction between resin and glass during cooling from the cure temperature.
6. It is possible to take account flow (due to plasticisation by water, for example) when computer modelling the self-stress fields in composites.
7. Using measured differences in the magnitudes of radial and tangential principal stresses, it appears that computer modelling of the true (inhomogeneous) self-stress fields of wet composites is feasible.

REFERENCES

Adams, D.F., (1979). 2nd Annual Army Composite Materials Research Review, 1-4 May 1979, University of Massachusetts, Amherst, Massachusetts. See also

Miller, A.K. and Adams, D.F., (1977) Departmental Report UWME-DR-7011111, "Micromechanical Aspects of Composite Materials", January 1977, Department of Mechanical Engineering, University of Wyoming, Laramie, Wyoming 82071.

Adams, D.F.,(1970). "Inelastic analysis of a unidirectional composite subjected to transverse normal loading." J. Composite Materials, 4, 310.

Alexander, J.M. and Turner, T.W.,(1975). "An investigation of the die-less drawing of titanium and some steels." 15th International M.T.D.R. Conference, Birmingham, England.

Ashbee, K.H.G., Frank, F.C., and Wyatt, R.C., 1967, Proc.Roy. Soc. Lond. A. 300, 415.

Ashbee, K.H.G., and Wyatt, R.C.,(1969) "Water damage in glass fibre/resin composites." Proc. R. Soc. A.,312,553

Cox, H.L., (1952). Br. J. Appl. Phys., 3, 72.

Durelli, A.J. and Riley, W.F., (1965) "Introduction to Photomechanics", Prentice-Hall Inc/Englewood Cliffs, N.J., 1965.

Farrar, N.R.,(1977) "Water damage in epoxy resin composites and adhesives" PhD Thesis, University of Bristol.

Gutfeld, R.J. von, and Melcher, R.L.,1977, Appl. Phys. Lett., 30, 257.

Kitson, N.K.,Low, S.A., and Turner, T.W. (1979). "Photoelastic visualisation experiments and a computer model for non-destructive testing." Ultrasonics International 79 Conference, Graz, Austria.

Poincaré H.,(1892). "Theorie mathematique de la lumière", II, Paris.

Slater, E.A., Baborovsky, V.M., and Marsh, D.M. (1975). Proceedings of the Ultrasonics International Conference.

Sneddon, I.N., 1945, Proc.Roy.Soc.Lond. A. 187, 229.

Turner, M.J., Clough, R.W., Martin, H.C., and Topp, L.J.,(1956),
"Stiffness and deflection analysis of complex structures." J. Aero. Sci.,
23, 805.

Wyatt, R.C.,(1975)"Imaging ultrasonic probe beams in solids."Br. J. non-destr. Test.,17,133-140.

Zienkiewicz, O.C.,(1977), "The finite element method" McGraw Hill.

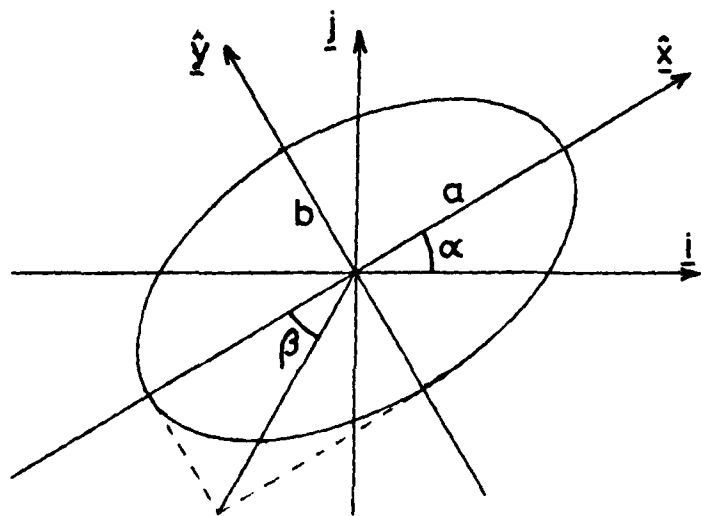


Figure 1. Projection of the E vector helix.

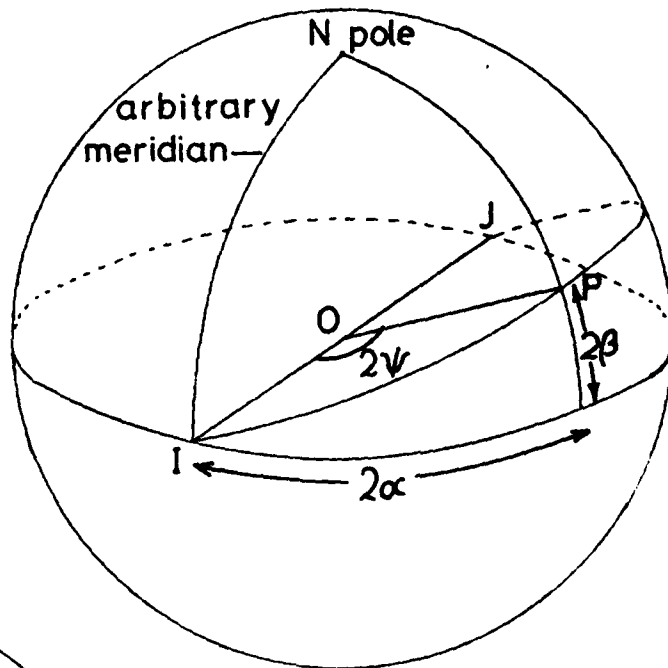


Figure 2. Poincaré sphere construction.

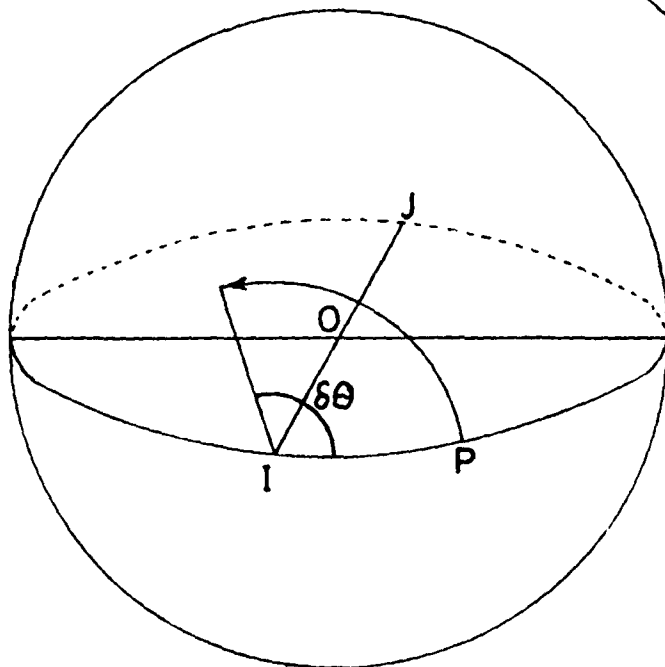


Figure 3. Effect of a retarder on elliptically polarized light.

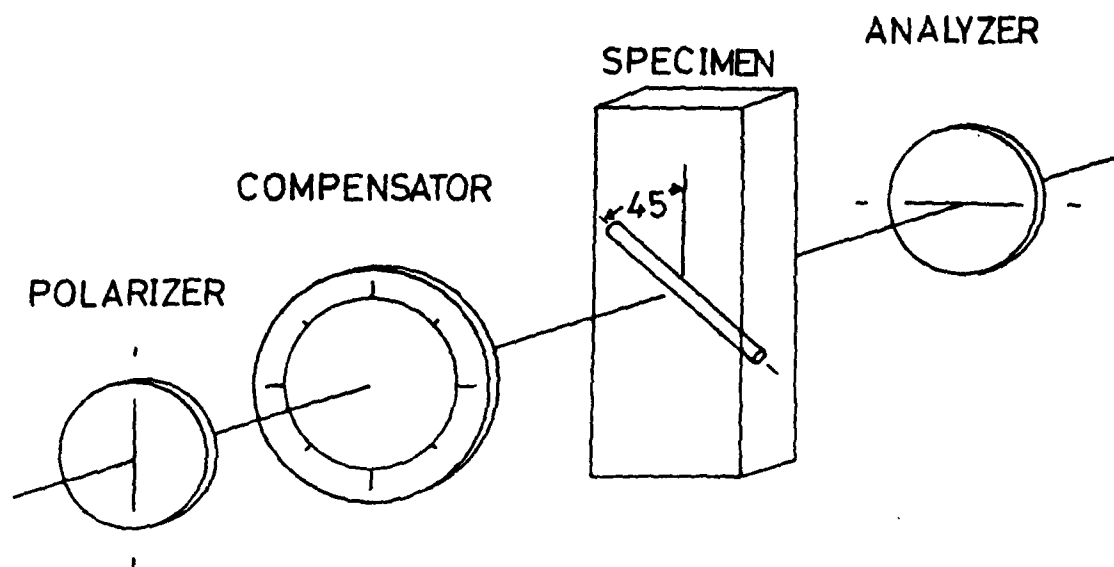


Figure 4. Typical experimental arrangement.

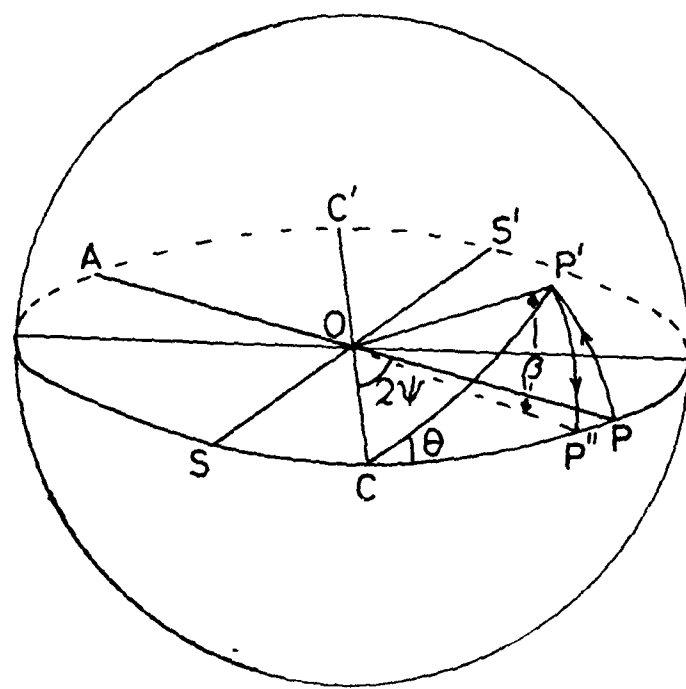


Figure 5. Poincaré sphere analysis of the above

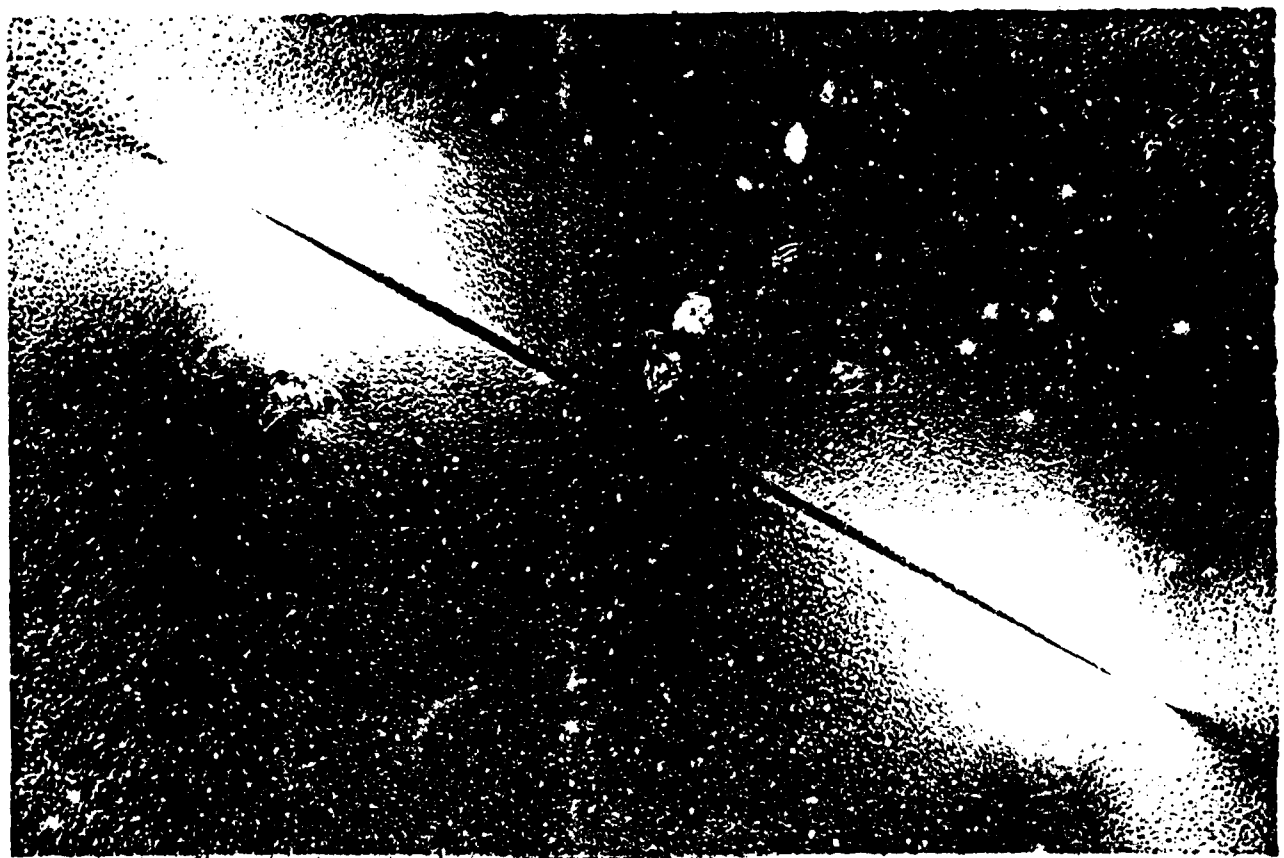


Figure 6 Stress induced birefringence in and around
an 'S' glass fibre drawn in ammonia.

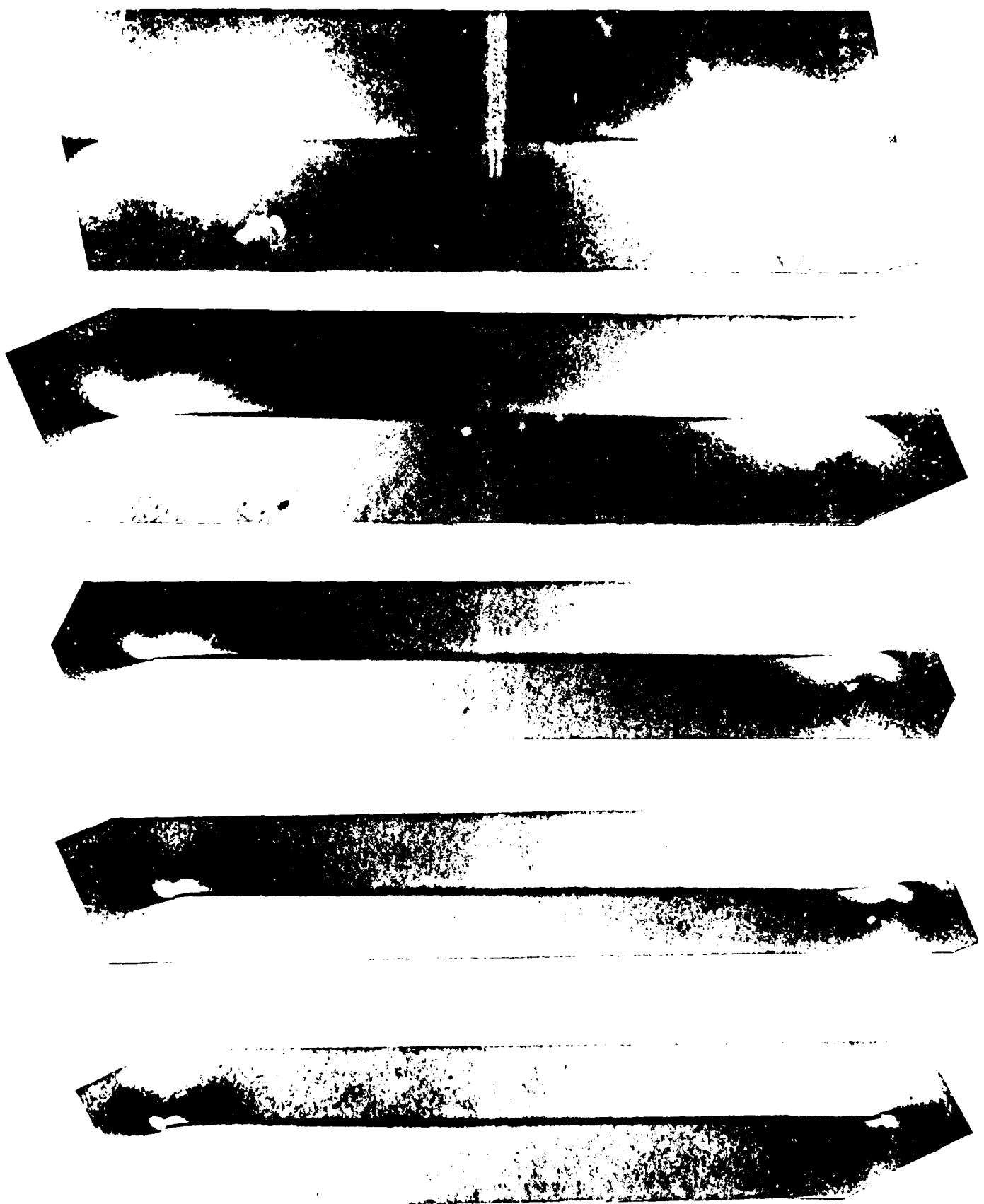


Figure 7 Series of photographs showing buildup
of shear stress.

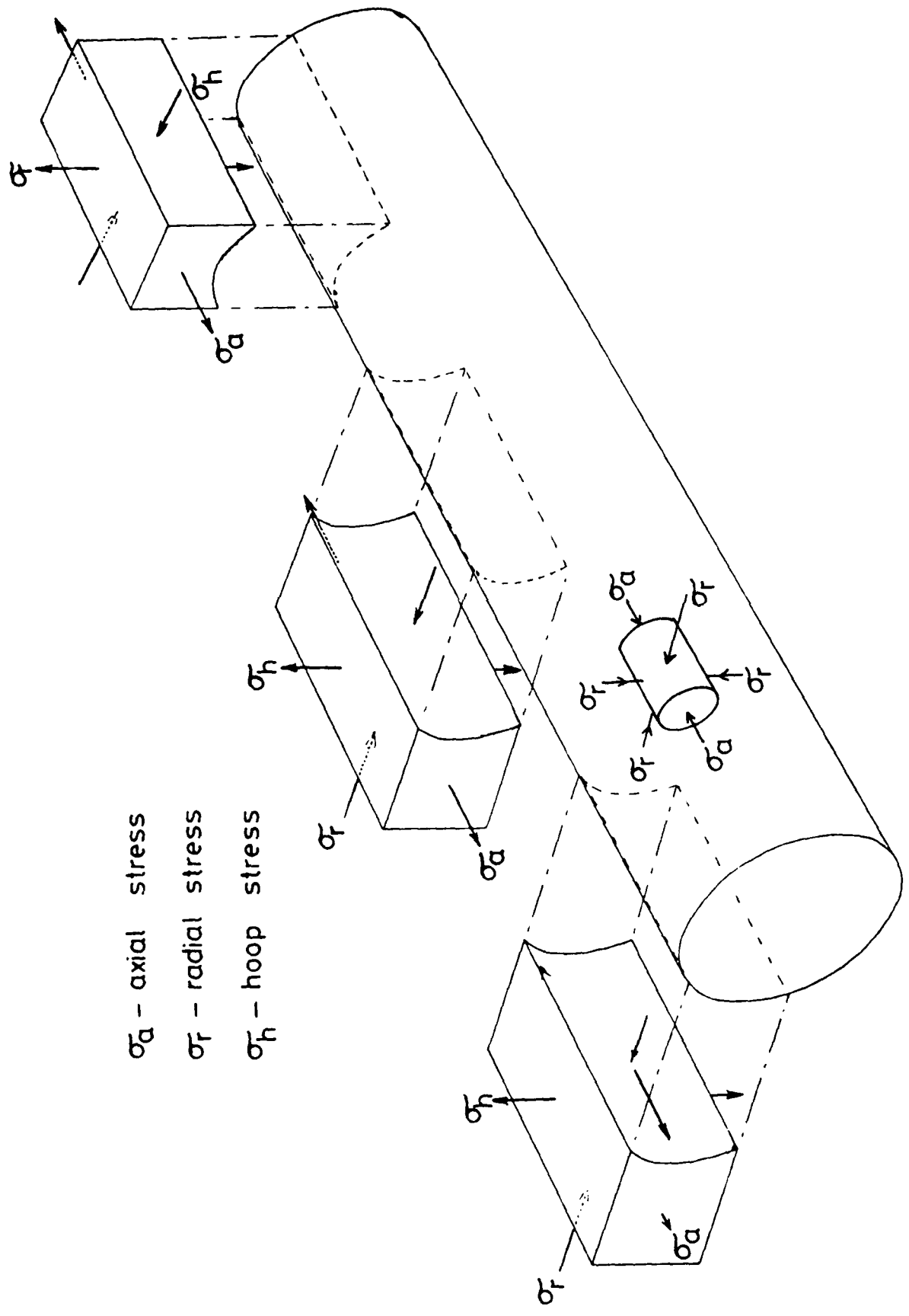


Figure 8 Schematic diagram showing the stresses in fibre and resin.

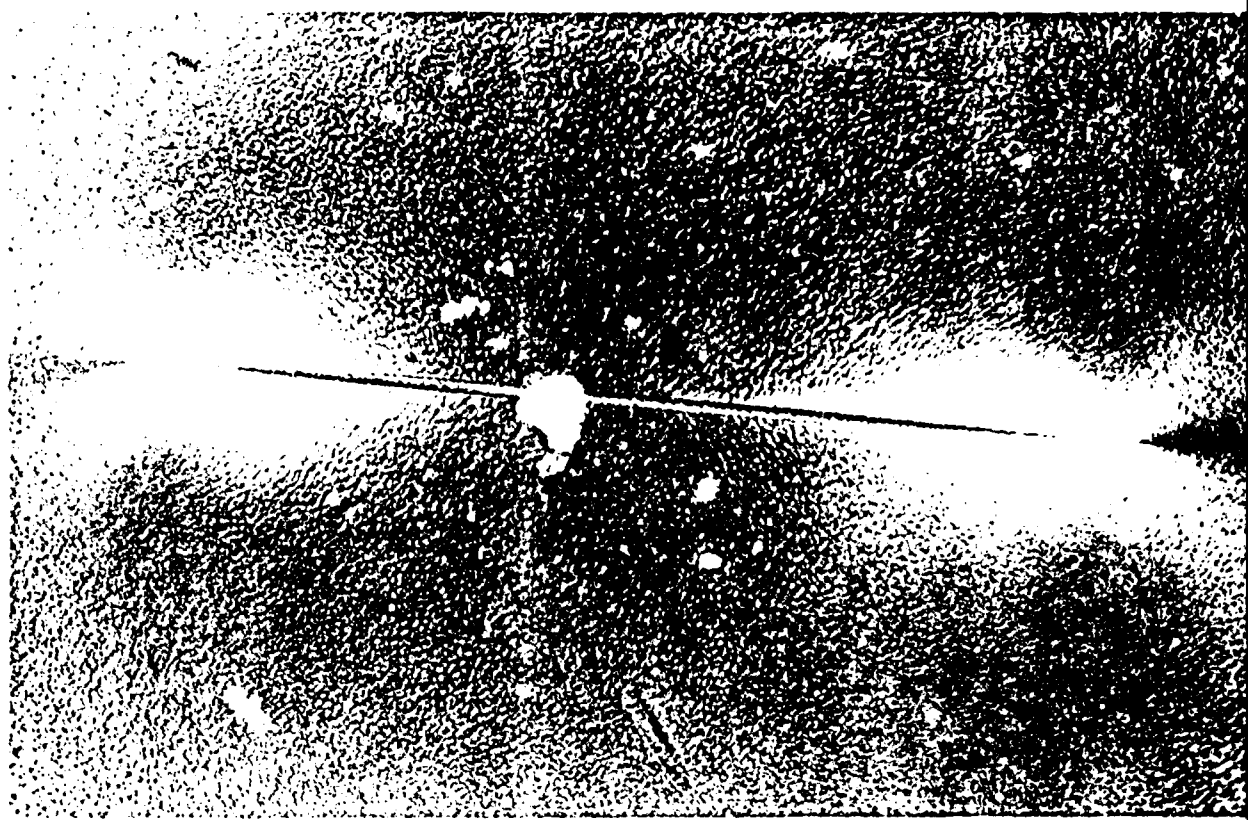


Figure 9 Isoclinics in and around a fibre misaligned
with the resin background birefringence.

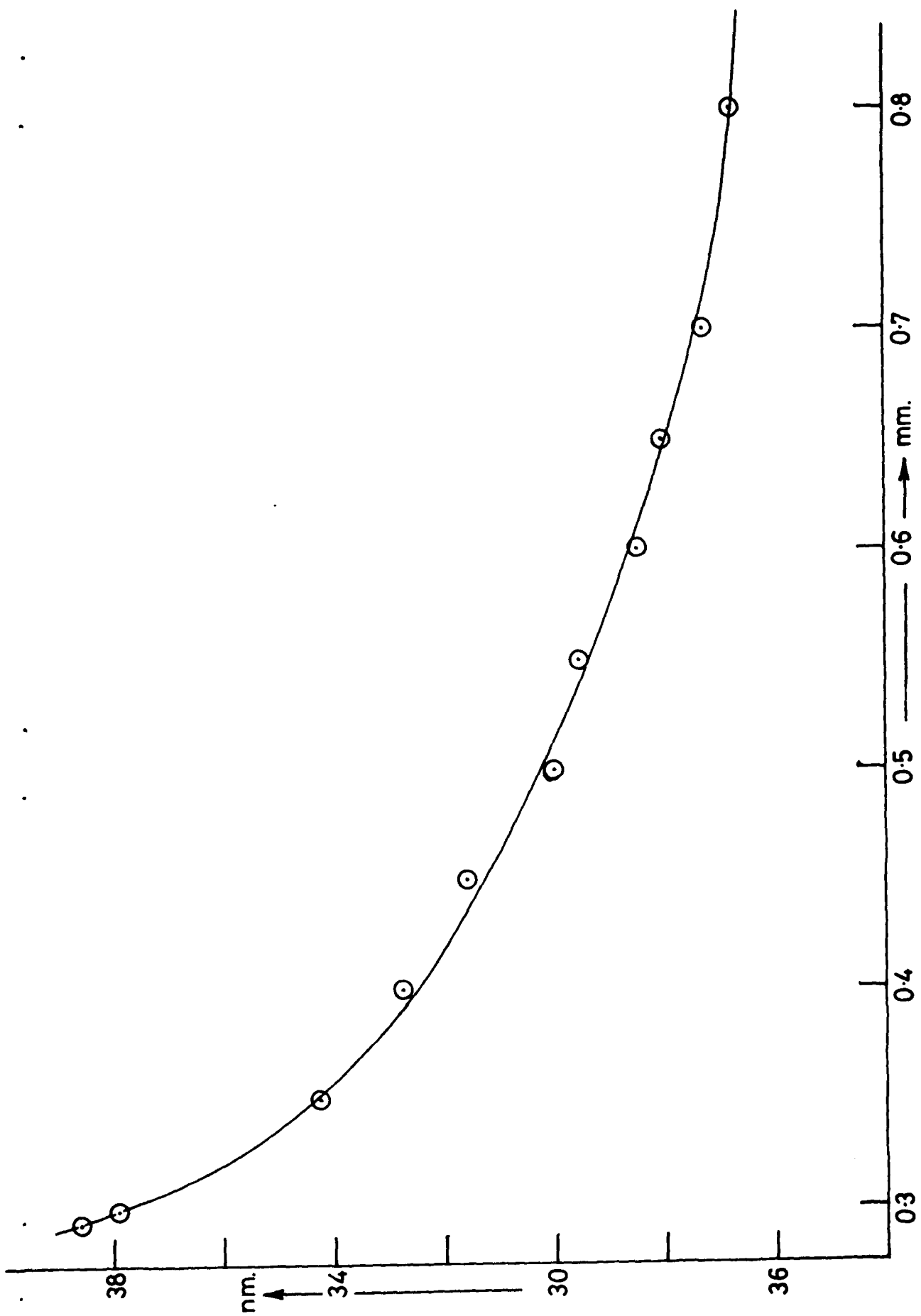


Figure 10 Retardation in resin vs. radial distance from fibre centre.

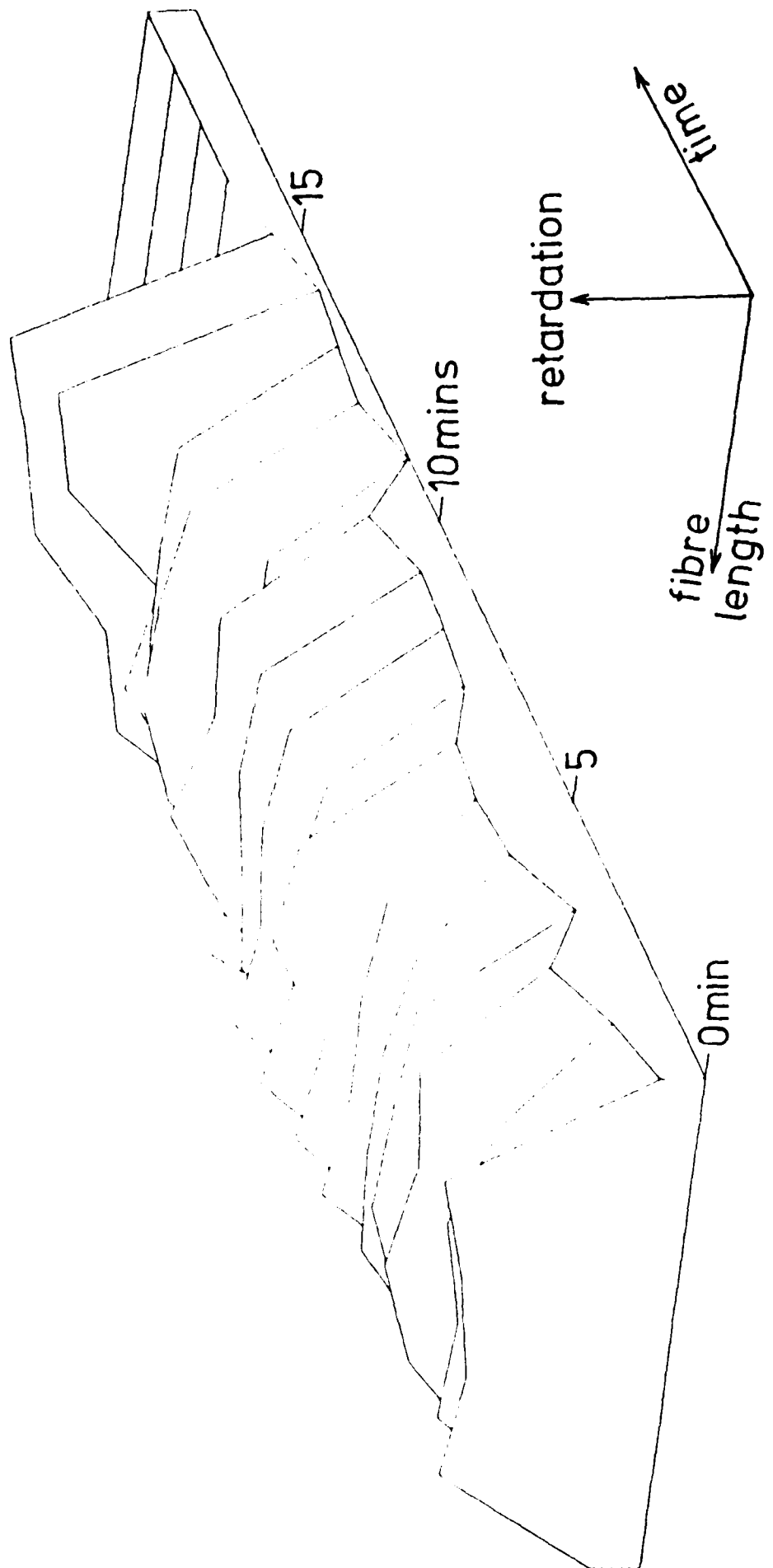


PLATE : 15G 00 ALTITUDE : 15000
DW : 60000 WEIGHT : 30000
BEFORE FORESHORTENING

Figure 11 Load transfer index - E glass - 100°C - 16 mins.

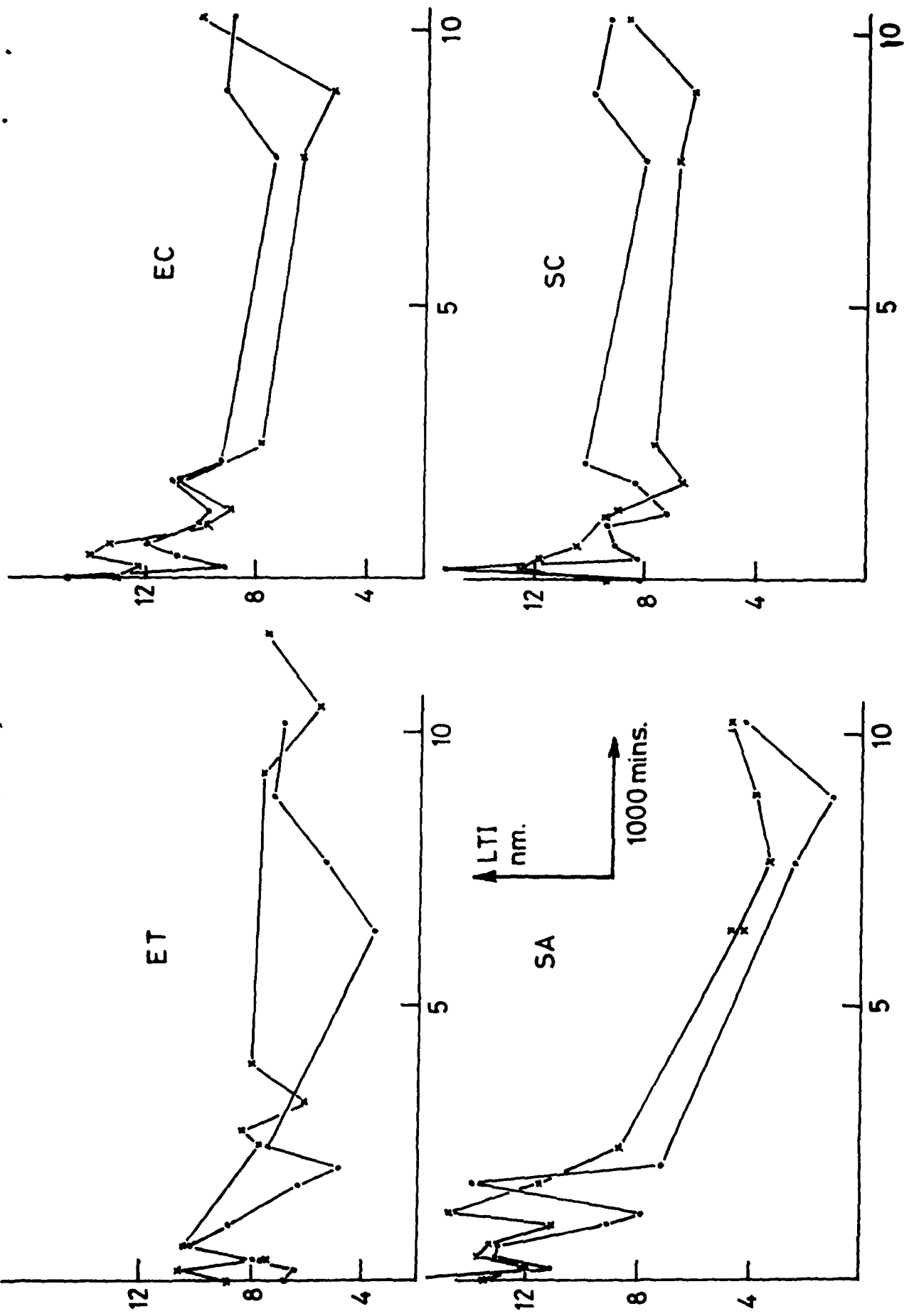


Figure 12 Load transfer index vs. immersion time for four glasses cast in MY 750 resin.

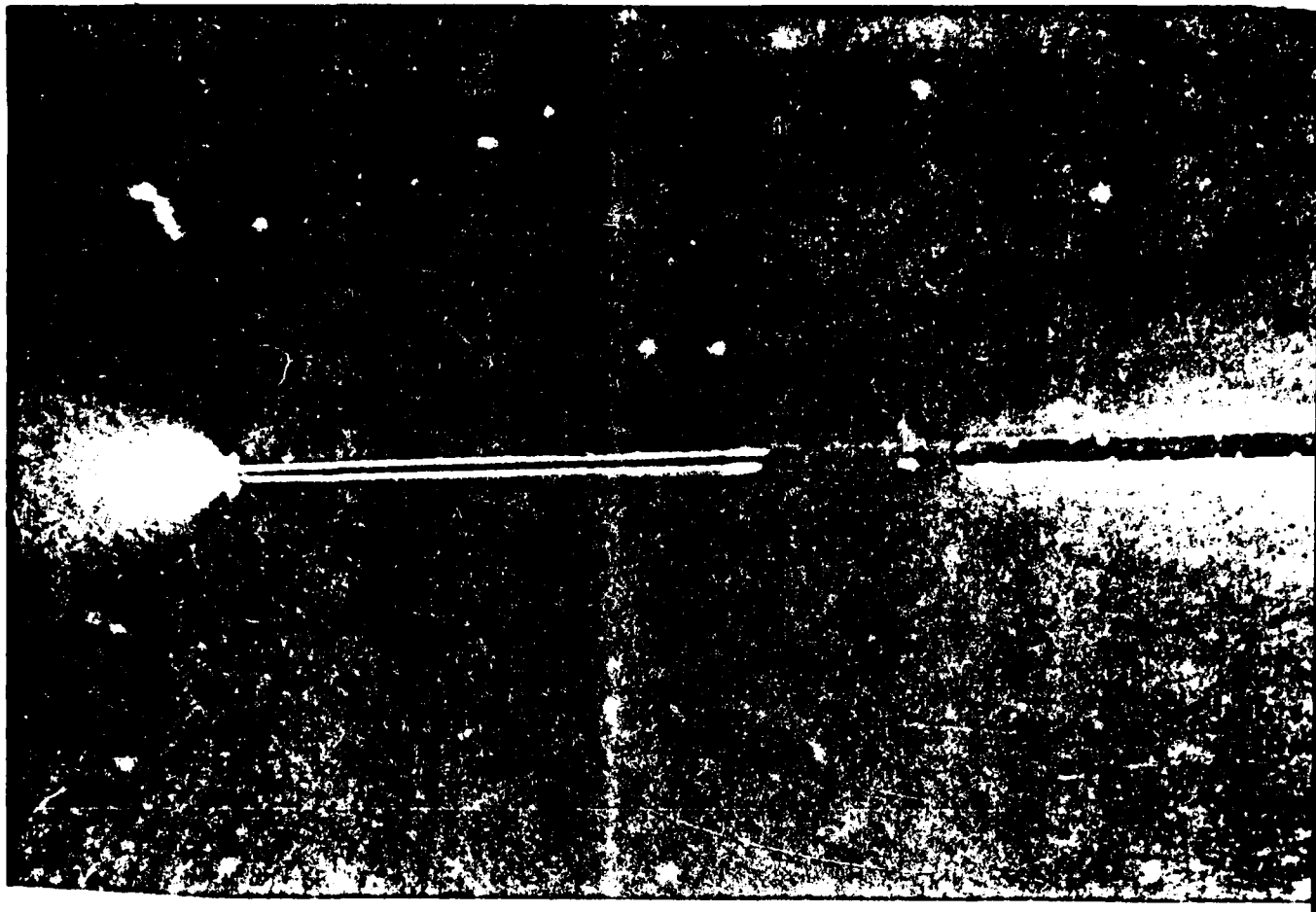


Figure 13 Photograph of an 'S' glass fibre drawn in ammonia, after
6400 minutes immersion in water at 60°C.

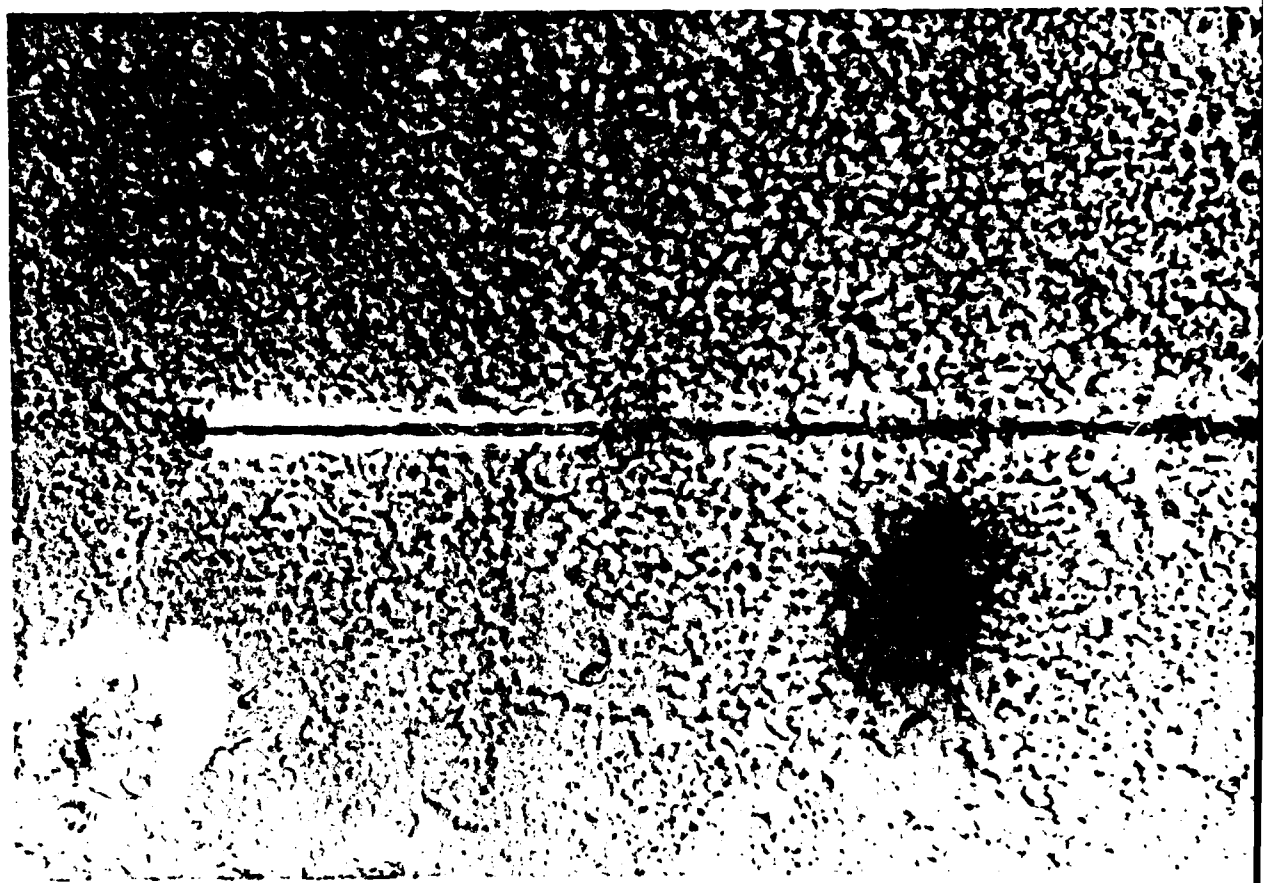


Figure 14 Photograph of an 'E' glass fibre drawn in ammonia, after
10200 minutes immersion in water at 60°C.

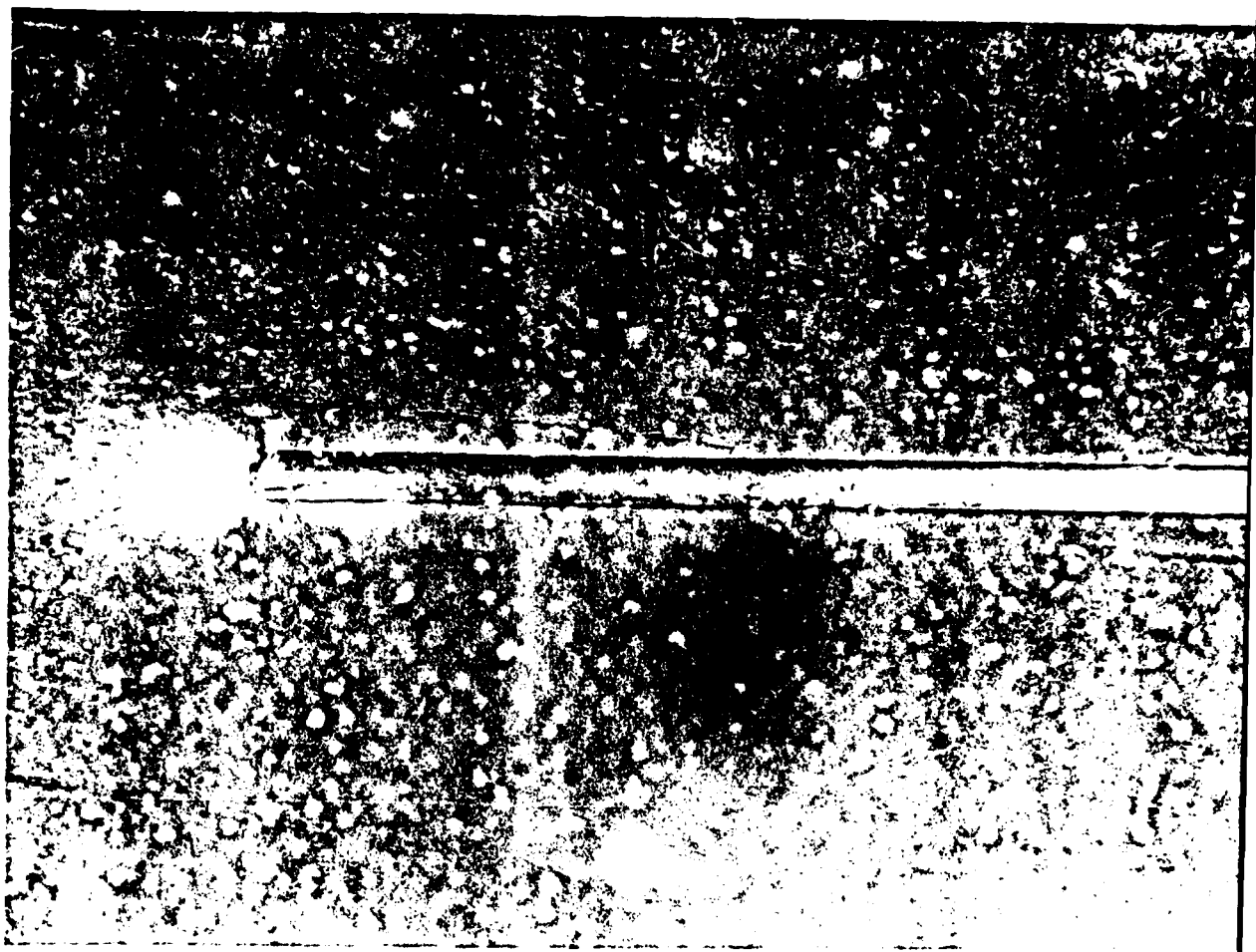


Figure 15 Photograph of a commercial 'S' glass fibre after
10200 minutes immersion in water at 60°C.

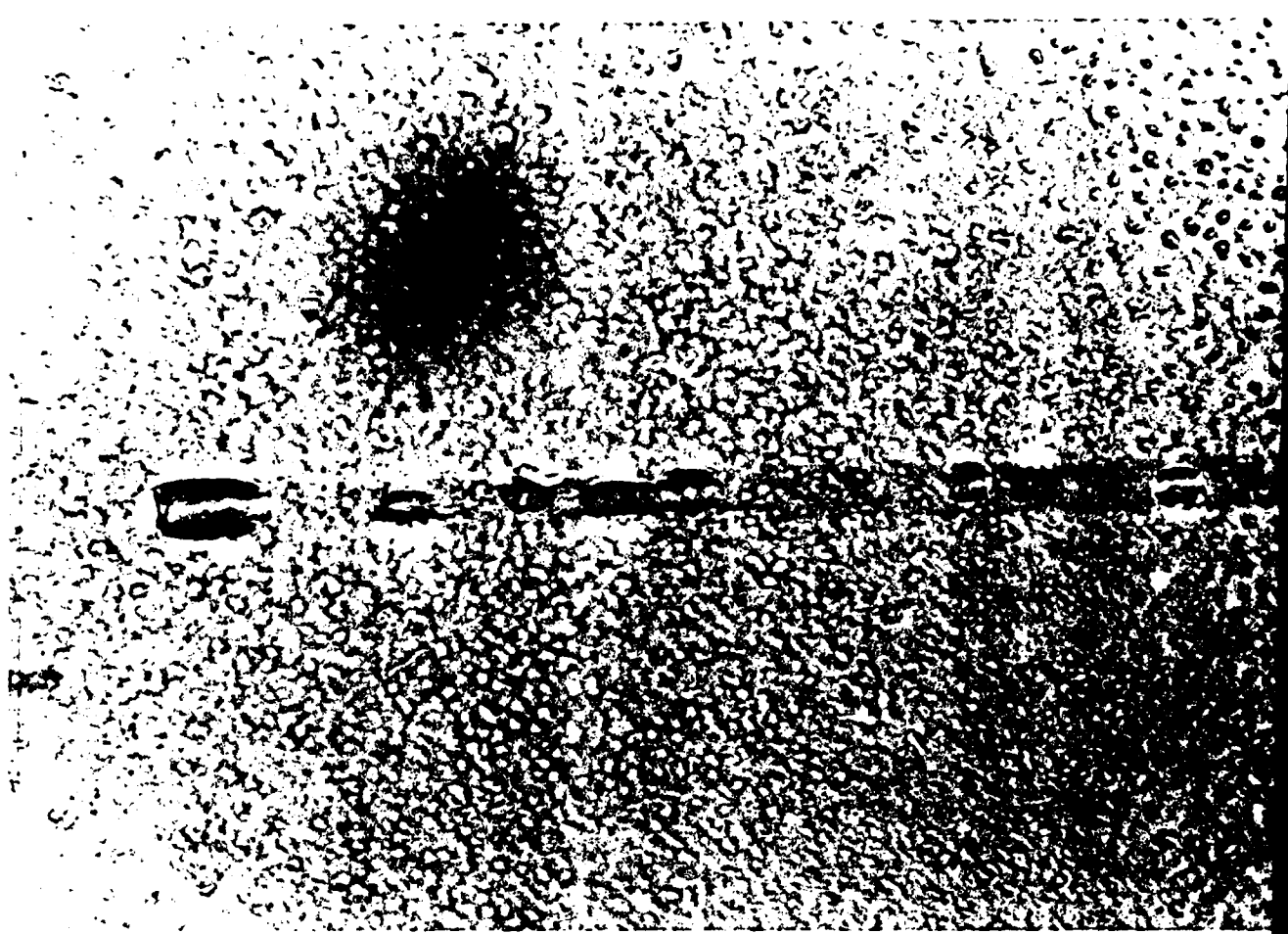


Figure 16 Photograph of a commercial 'E' glass fibre after
10200 minutes immersion in water at 60°C.

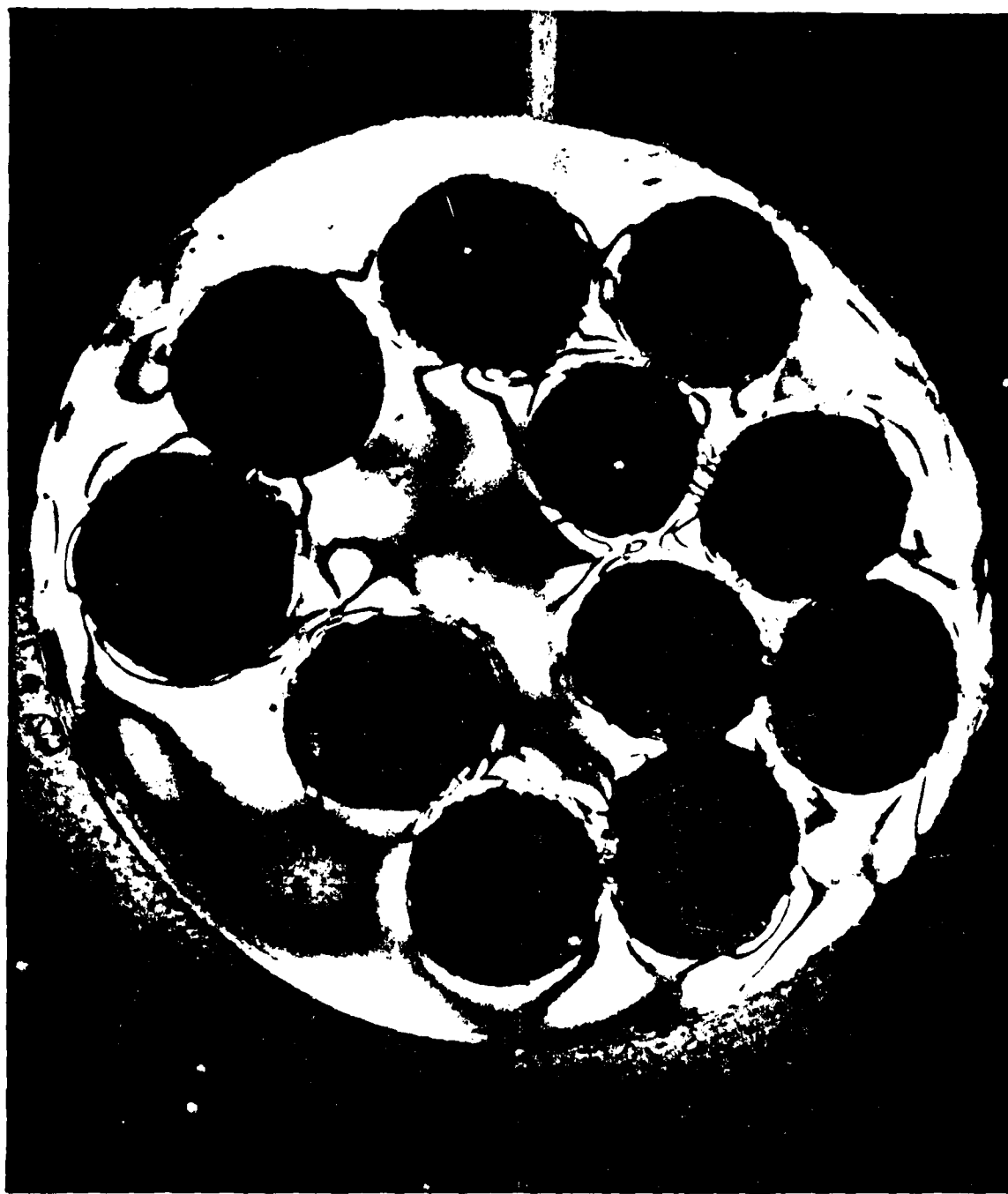


Figure 17 Photograph of a transverse section of a model unidirectional composite examined with the polarising microscope.

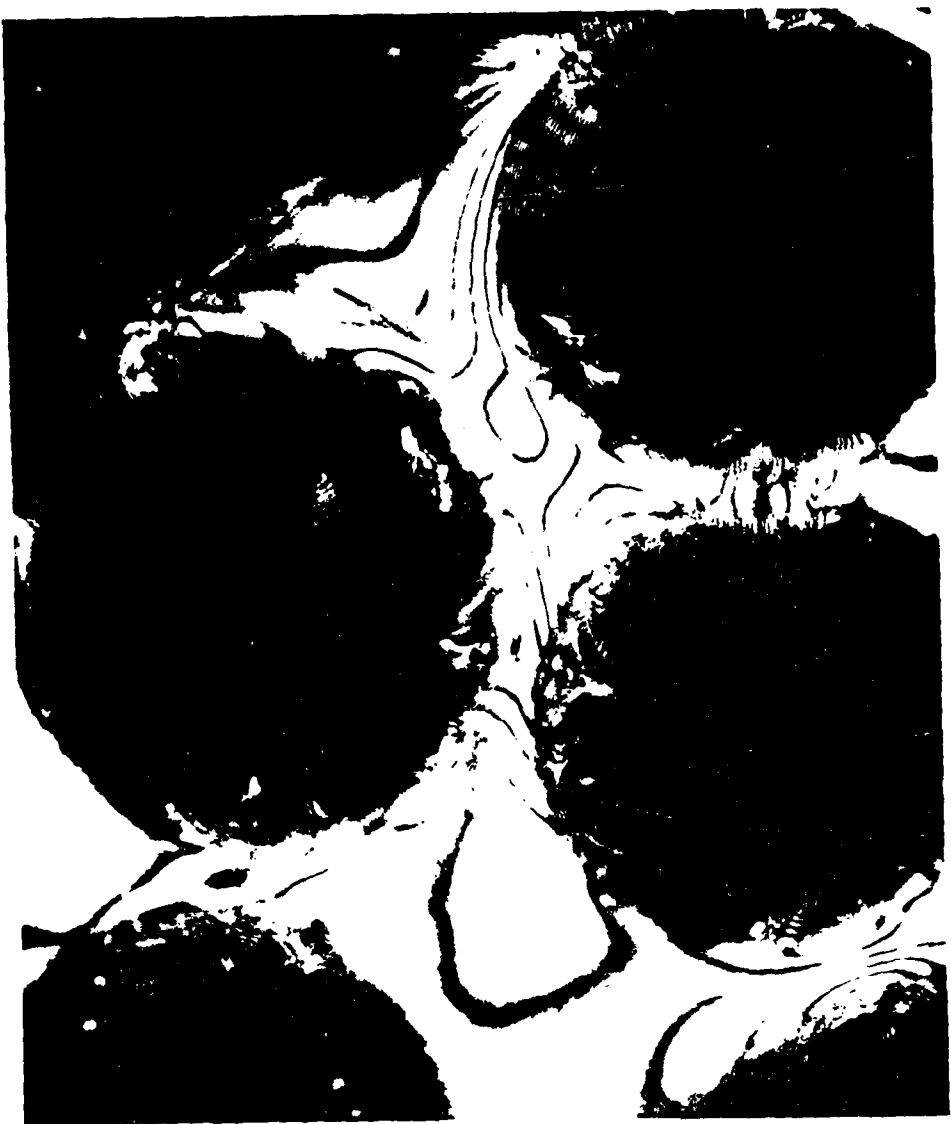
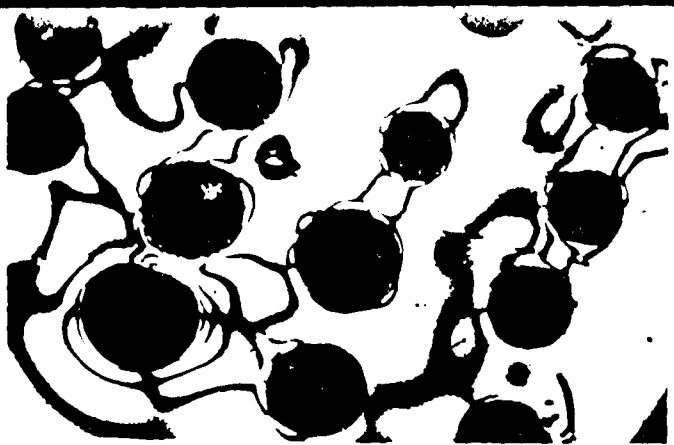


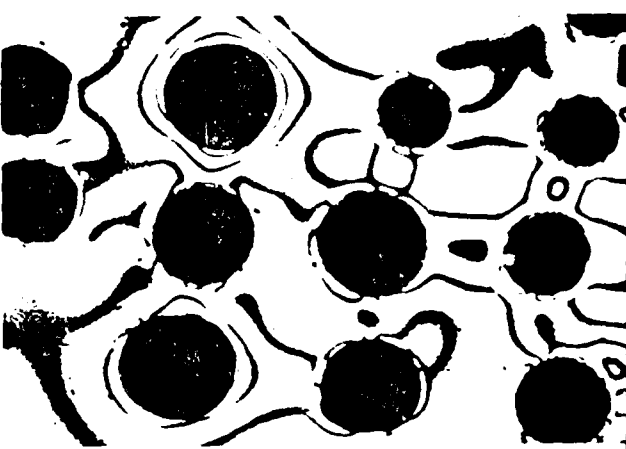
Figure 18 Photograph of a small region of a transverse section examined with polariser and analyser crossed.



2 mm



10 mm



16 mm

Isoclinics + isochromaticsIsochromatics

Figure 19 Photograph of transverse sections examined in both plane and circular polarised light. The fibres are arranged in a periodic array.



Figure 20 Photograph of a small region of a transverse section examined with polariser and analyser crossed.

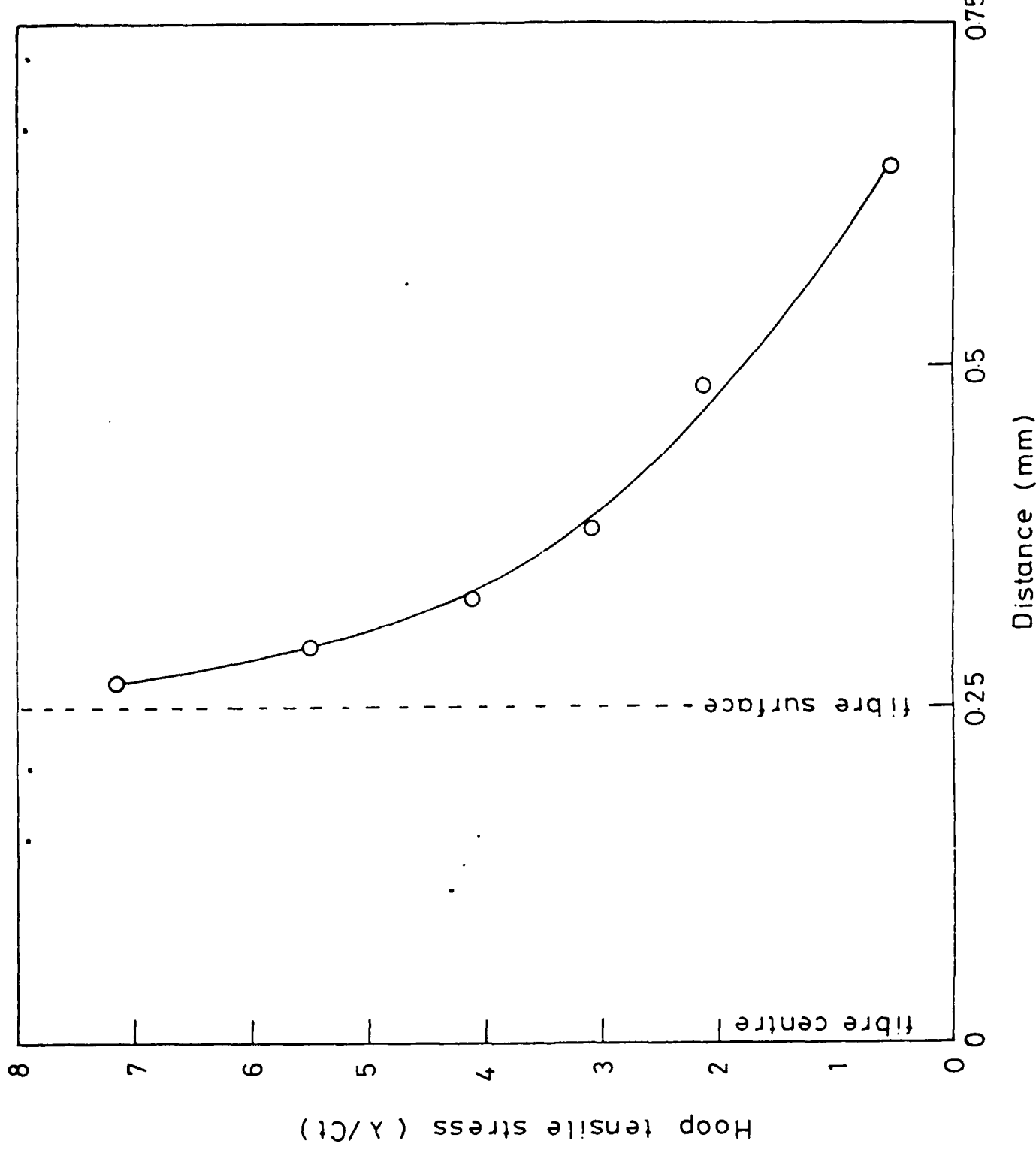


Figure 21 Plot of the hoop tensile stress against radial distance from the fibre.

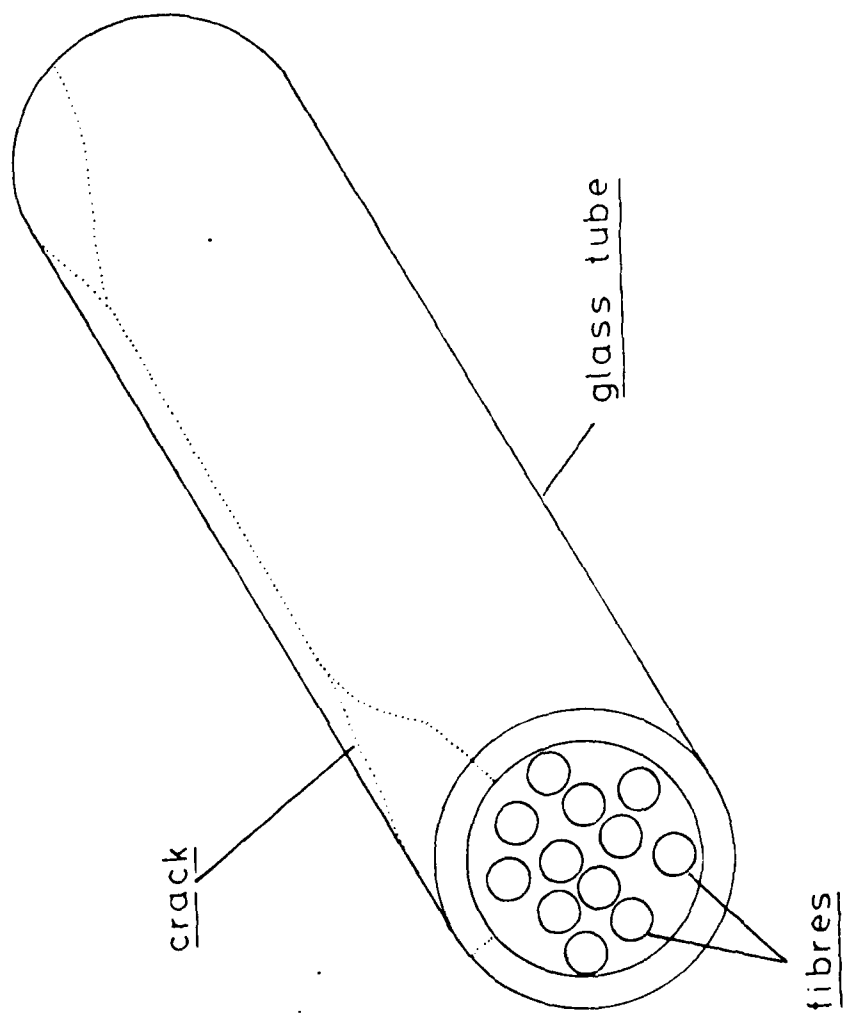
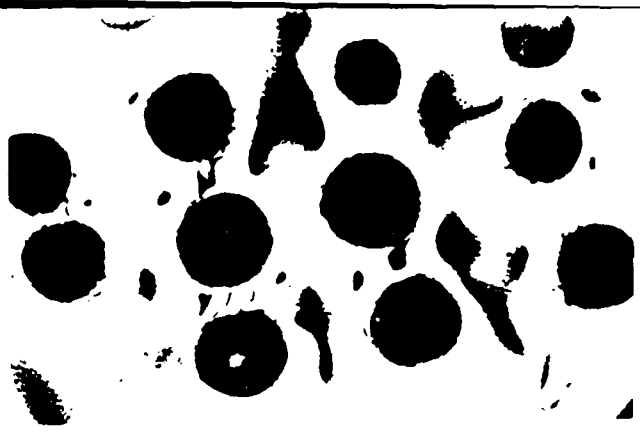


Figure 22 Schematic diagram showing the cracking of the glass tube in which the specimen was cast. After immersion in water at 80°C for 4 days.



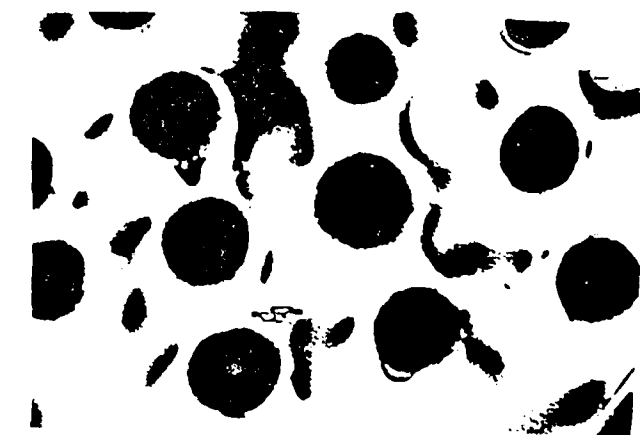
2 mm



10 mm



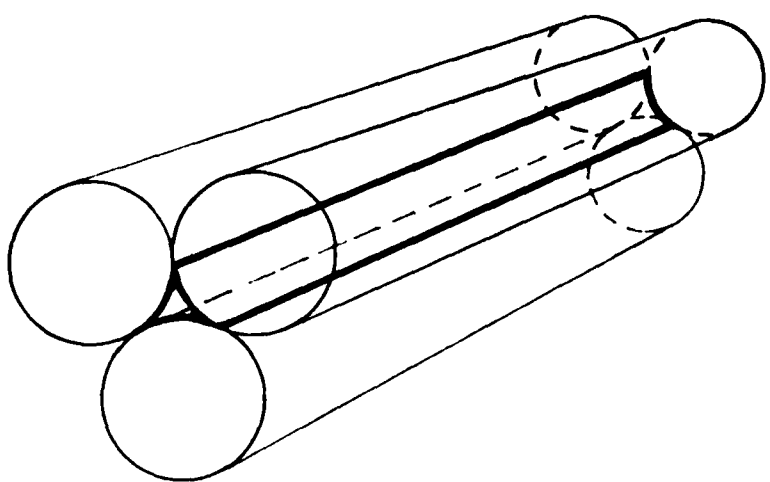
16 mm



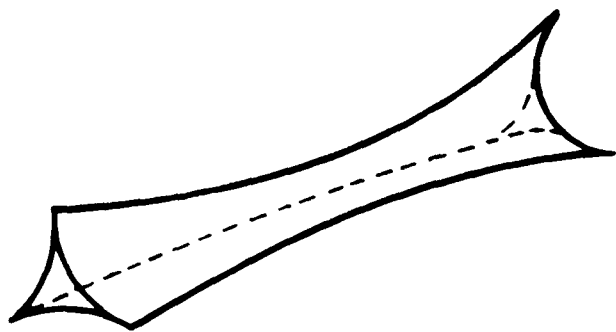
Isoclinics + isochromatics

Figure 23 Photograph of transverse sections examined in plane and circularly polarised light .After immersion in water at 80°C for 4 days.
The fibres are arranged in a periodic array.

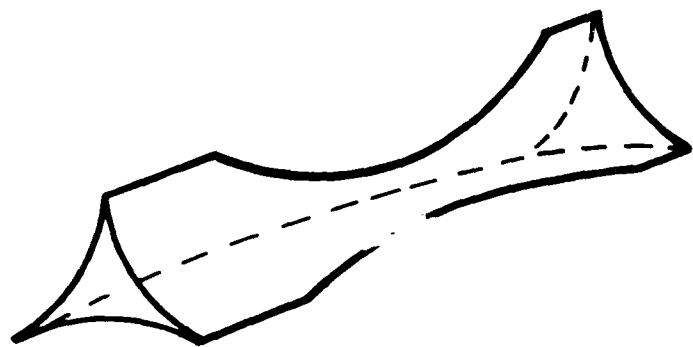
Isochromatics



(A)



(B)



(C)

Figure 24

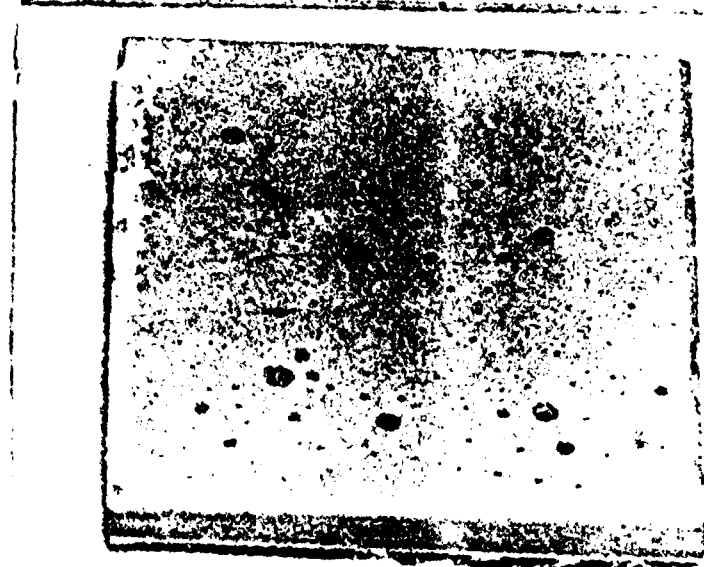
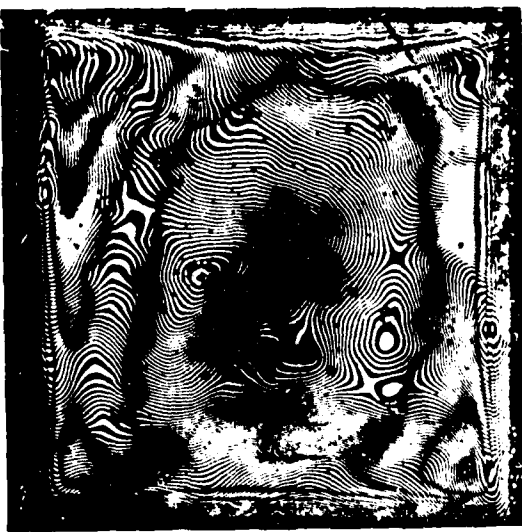


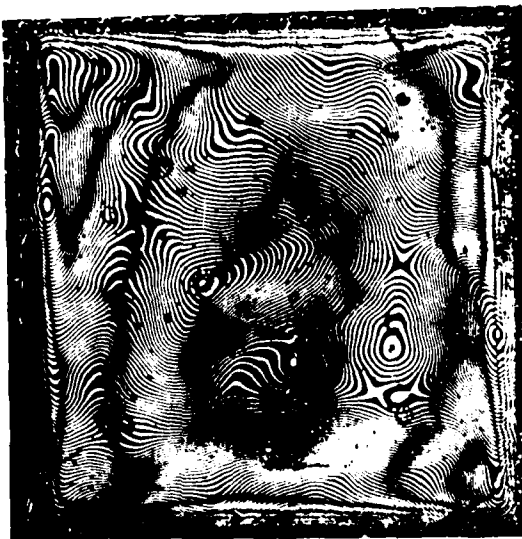
Figure 25



8 Hrs



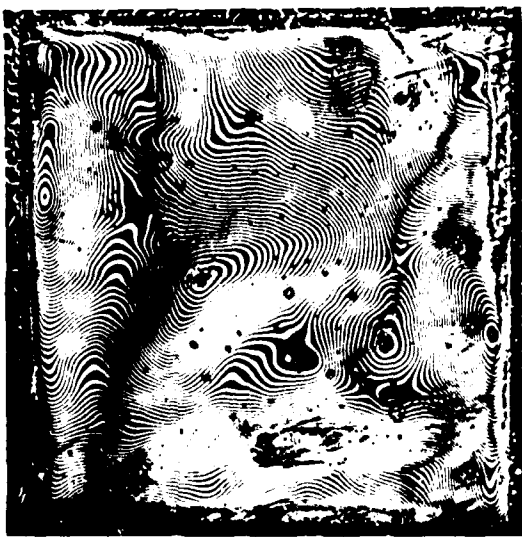
167 Hrs



5 Hrs



81 Hrs



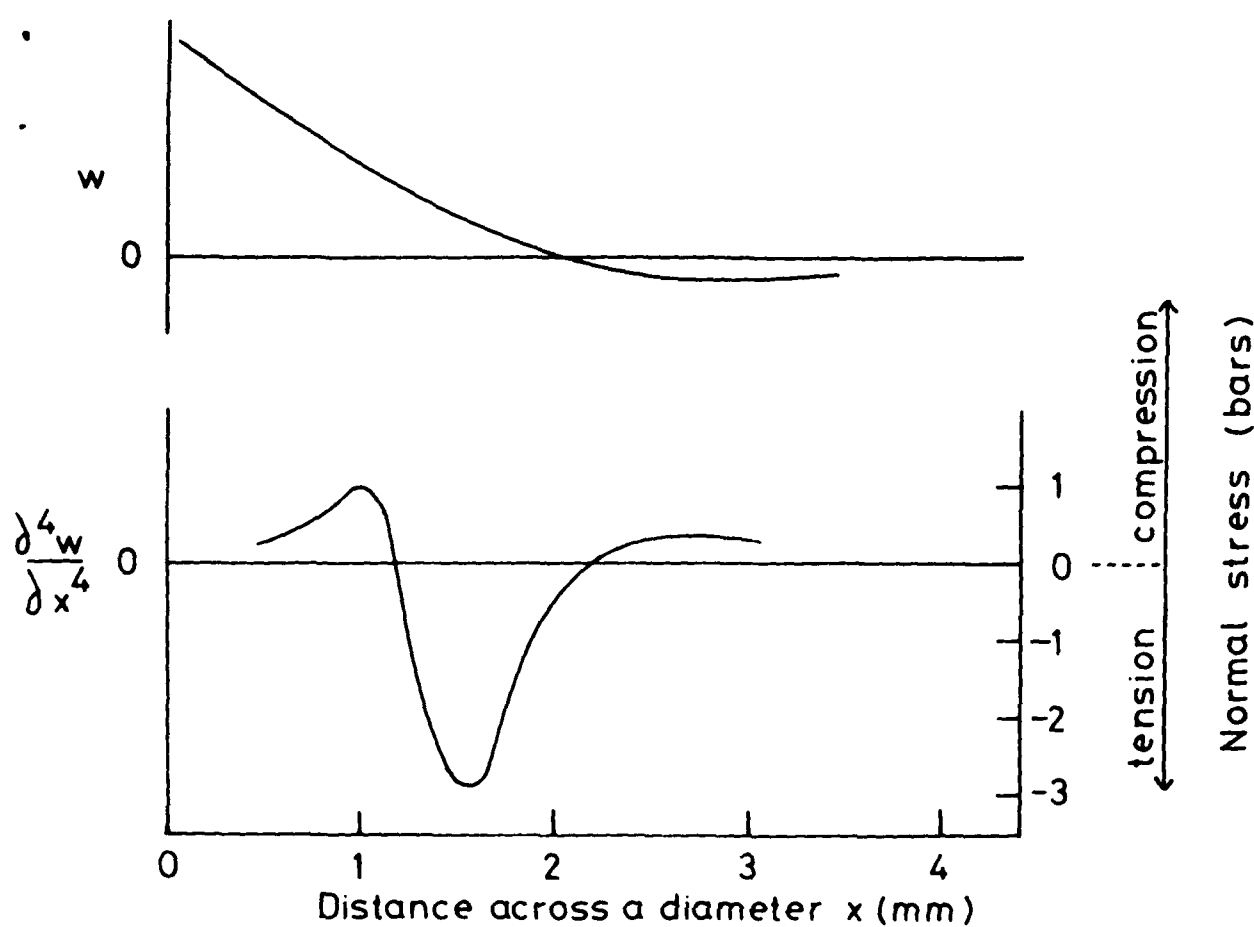
1 Hr



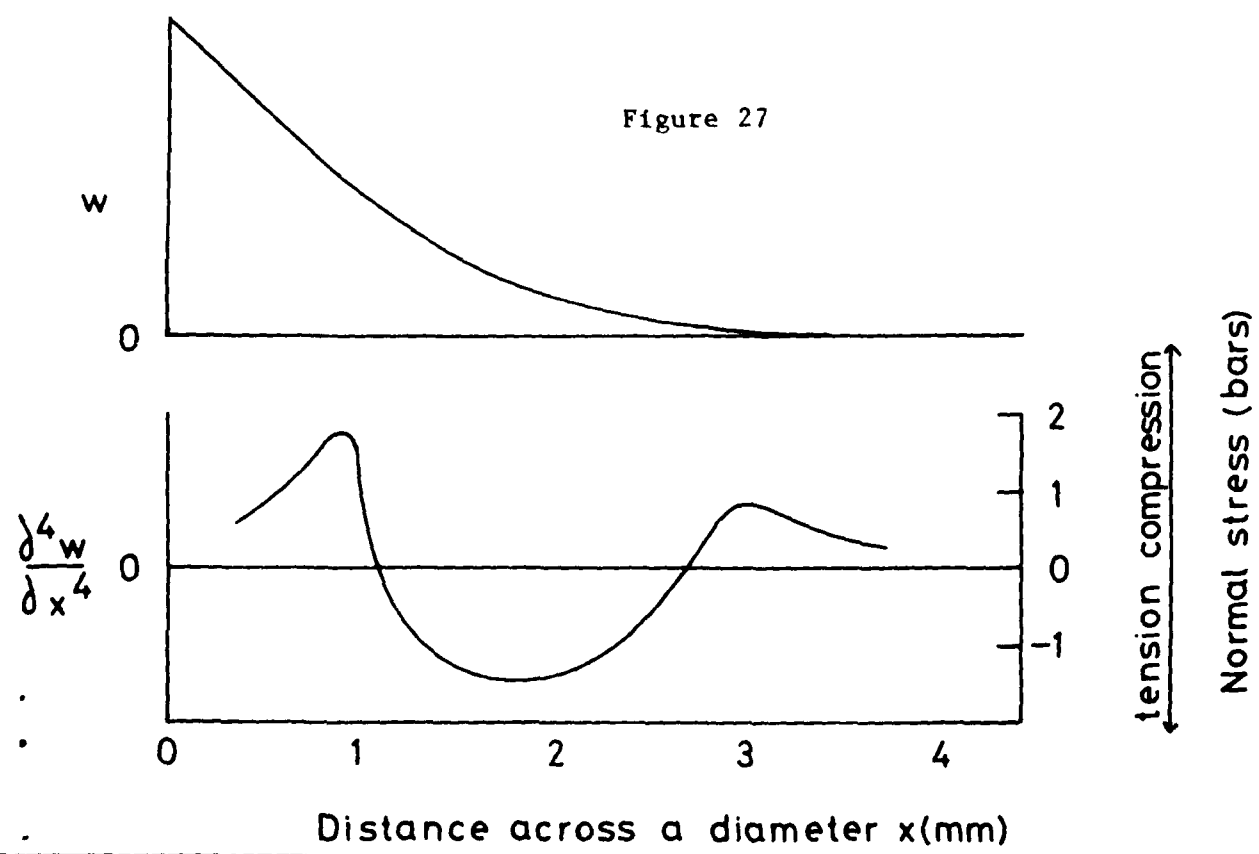
22 Hrs

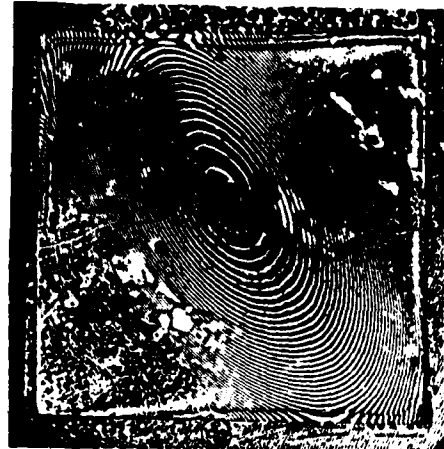
Figure 26

Across the fibres

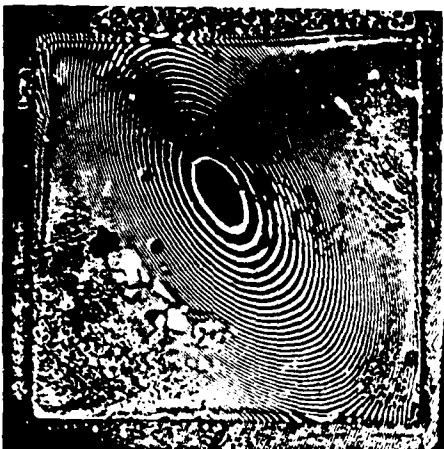


Parallel to the fibres

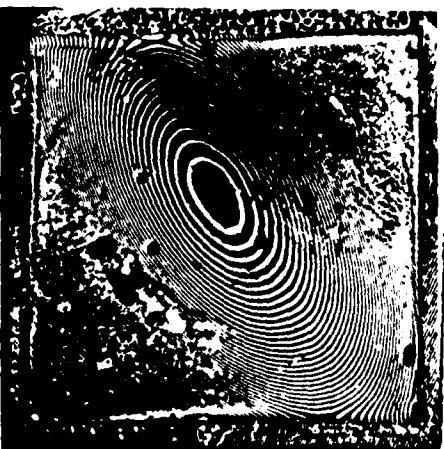




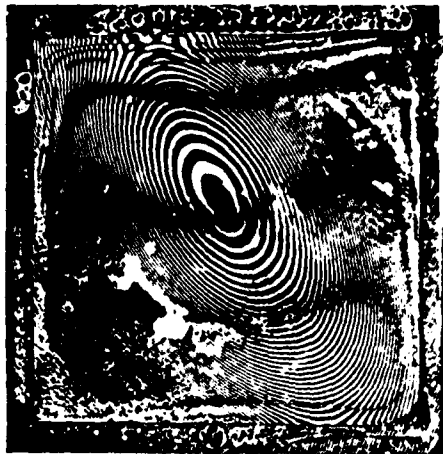
6.5 Hrs



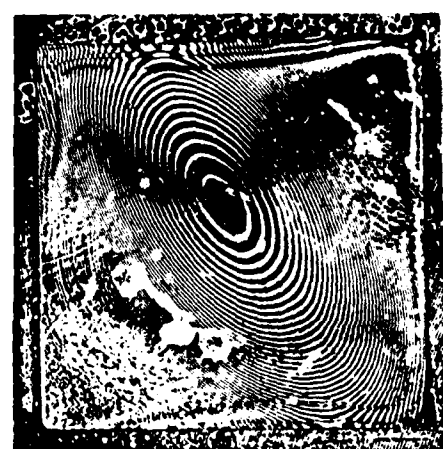
23 Hrs



31 Hrs



72 Hrs



144 Hrs

Figure 28 Moire patterns for MY 750 resin immersed in water at 60°C showing the ingress of swelling during water uptake.

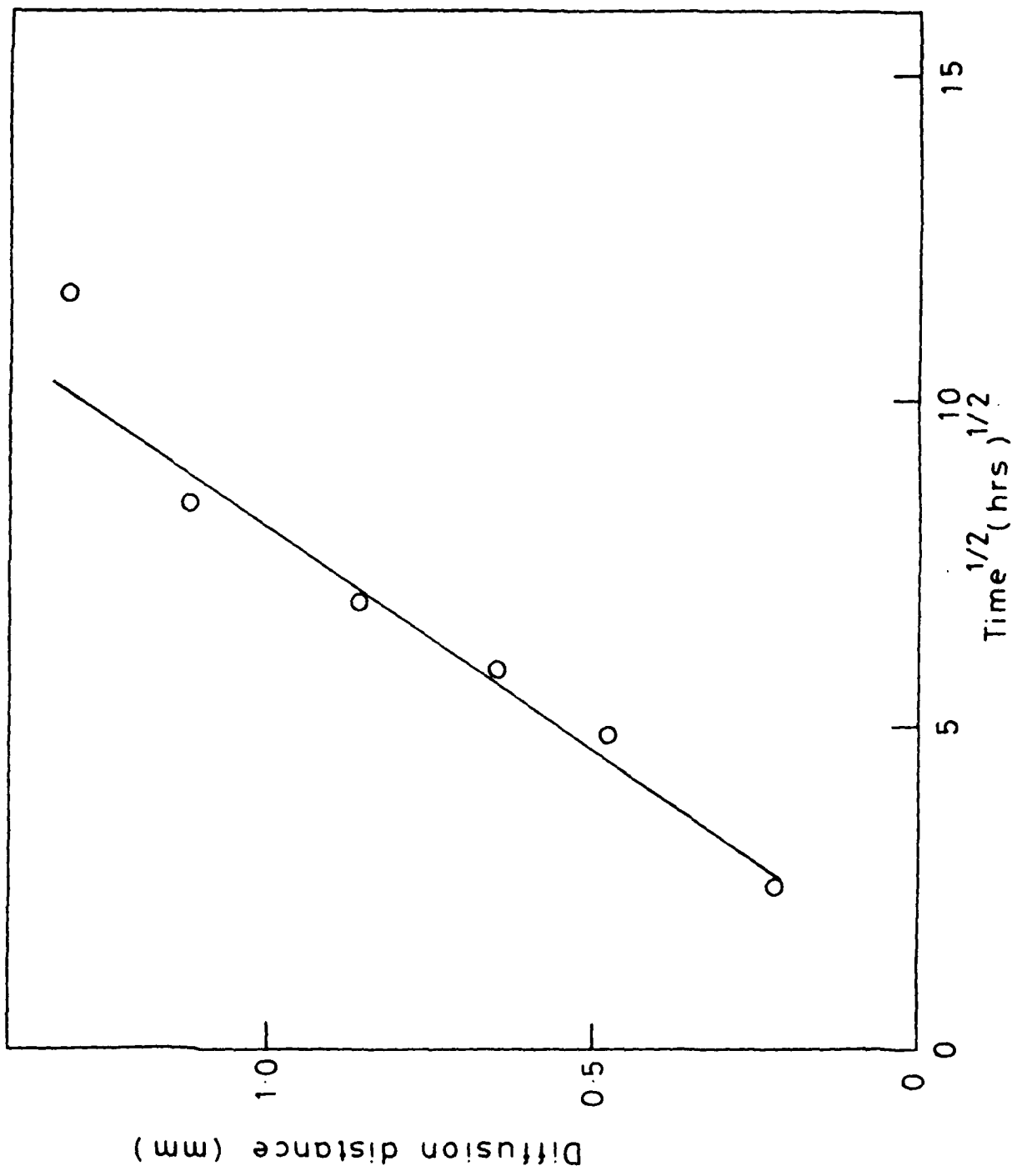


Figure 29 Migration distance of the 1st Moiré fringe, shown in figure 6, plotted against the square root of time.

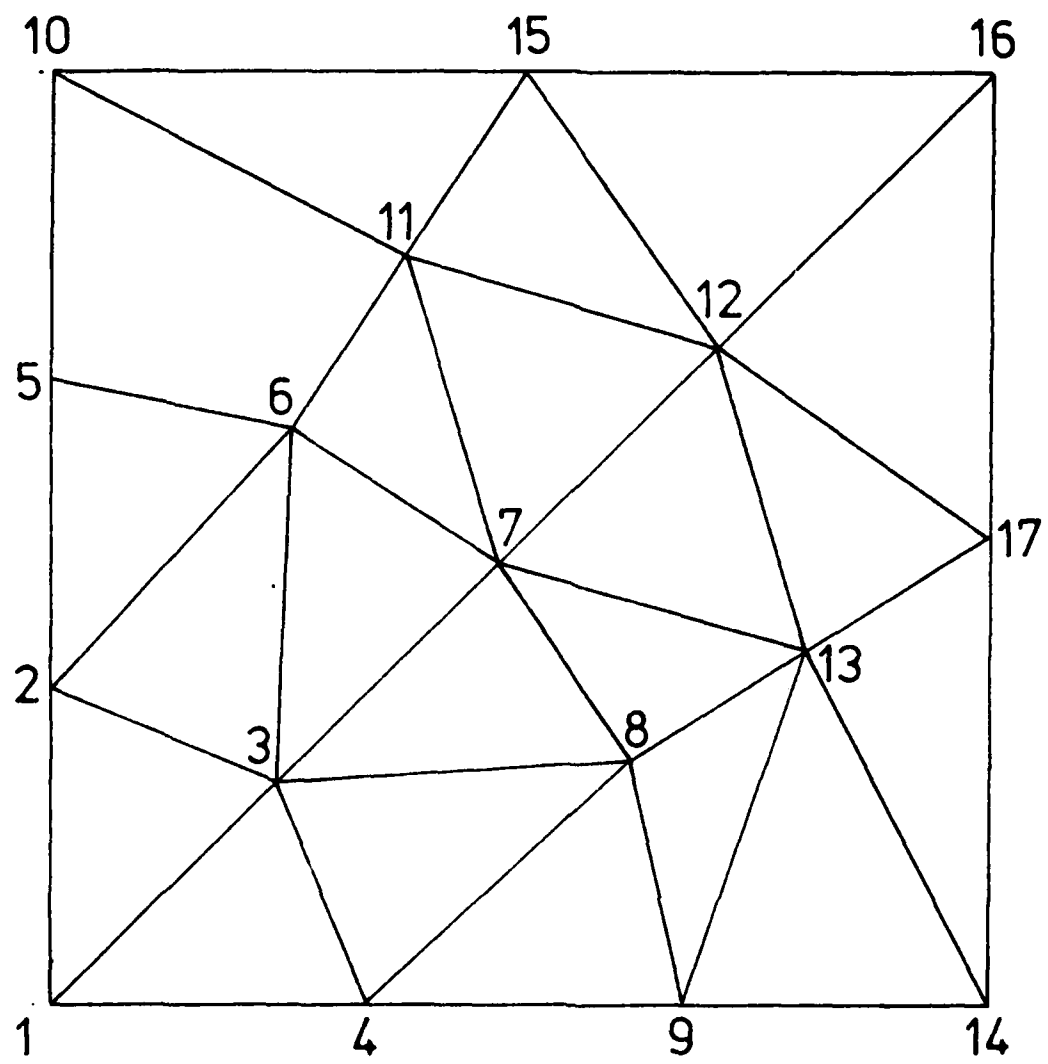


Figure 30 22-element mesh

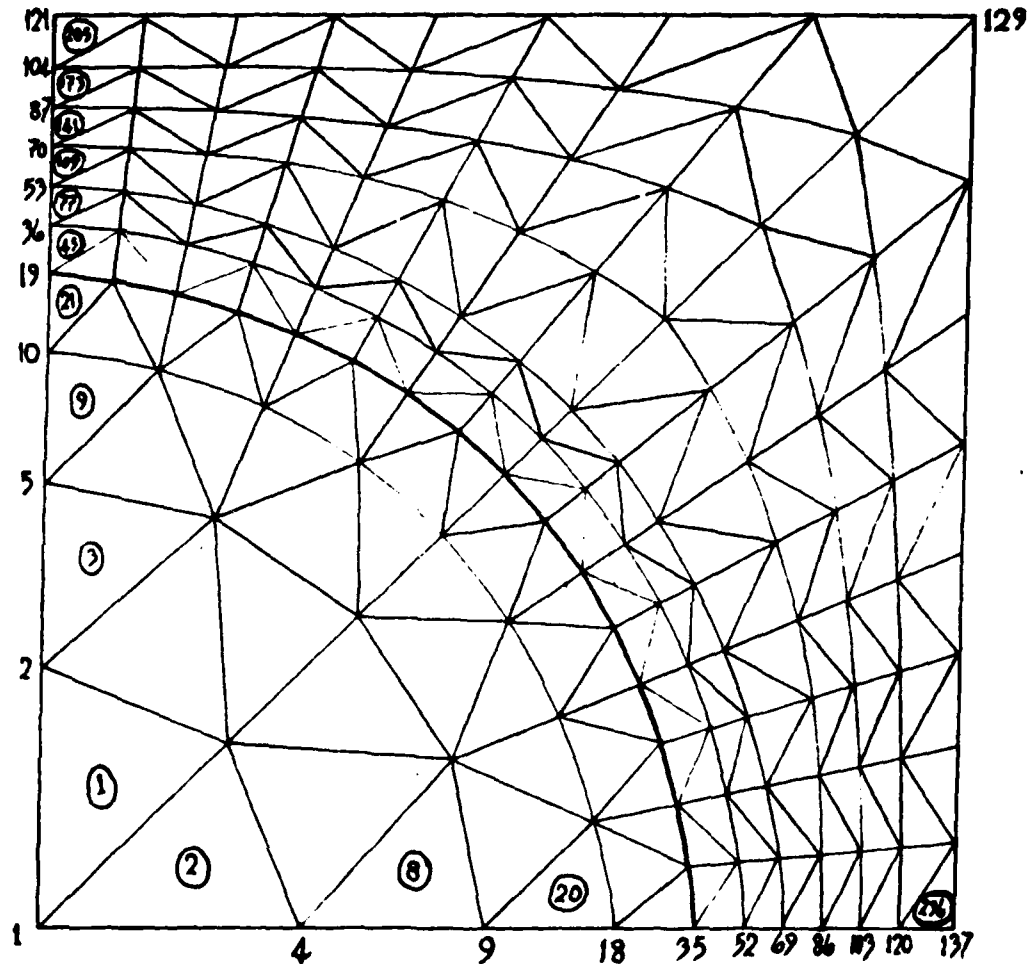


Figure 31 236-element mesh

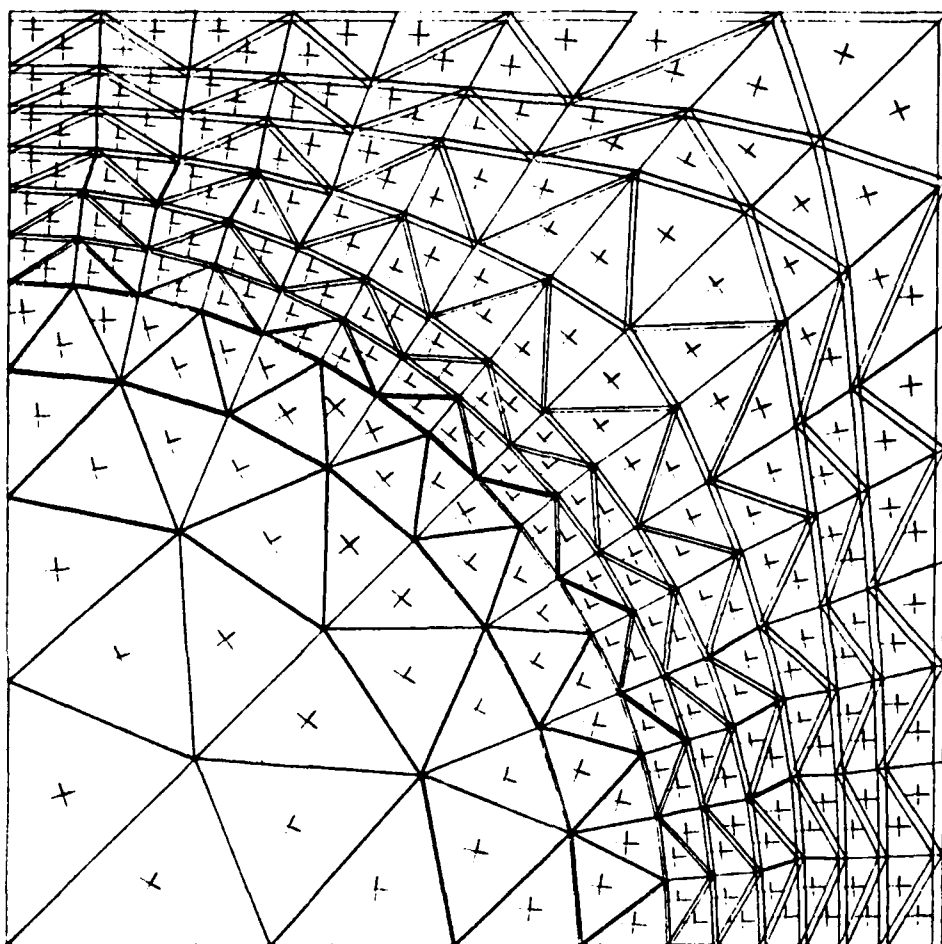


Figure 32 1% Biaxial tensile strain, small fibre,
low plasticity interface.

Stresses in element 1 are: 96.7 M Pa and 96.9 M Pa.

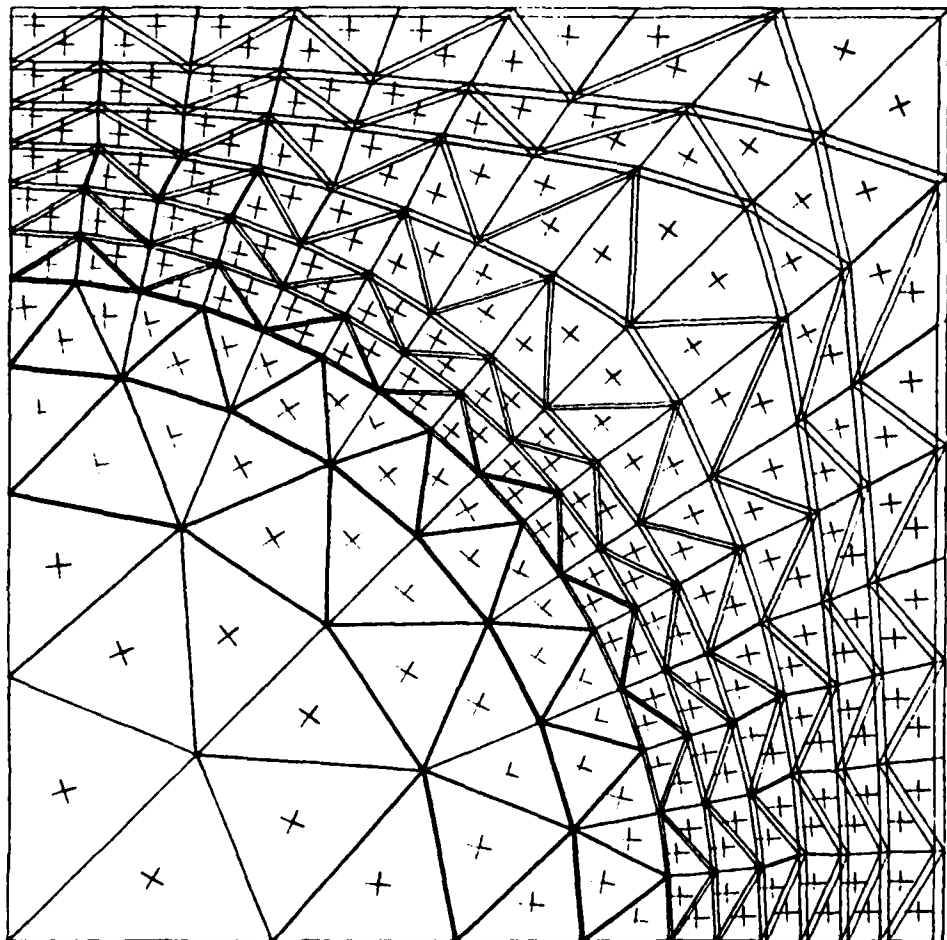


Figure 33 1% Biaxial tensile strain, small fibre,
high plasticity interface.

Stresses in element 1 are: 93.1 M Pa and 93.3 M Pa.

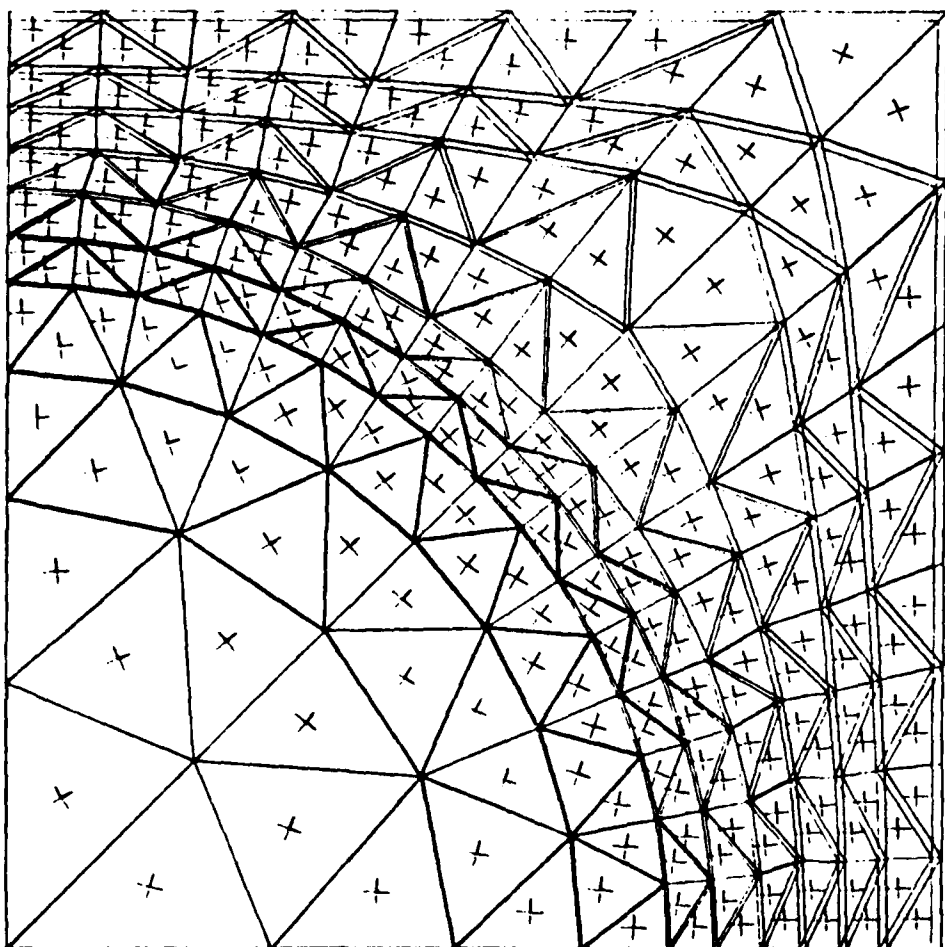


Figure 34 1% Biaxial tensile strain, large fibre,
low plasticity interface.

Stresses in element 1 are: 145 M Pa and 145 M Pa.

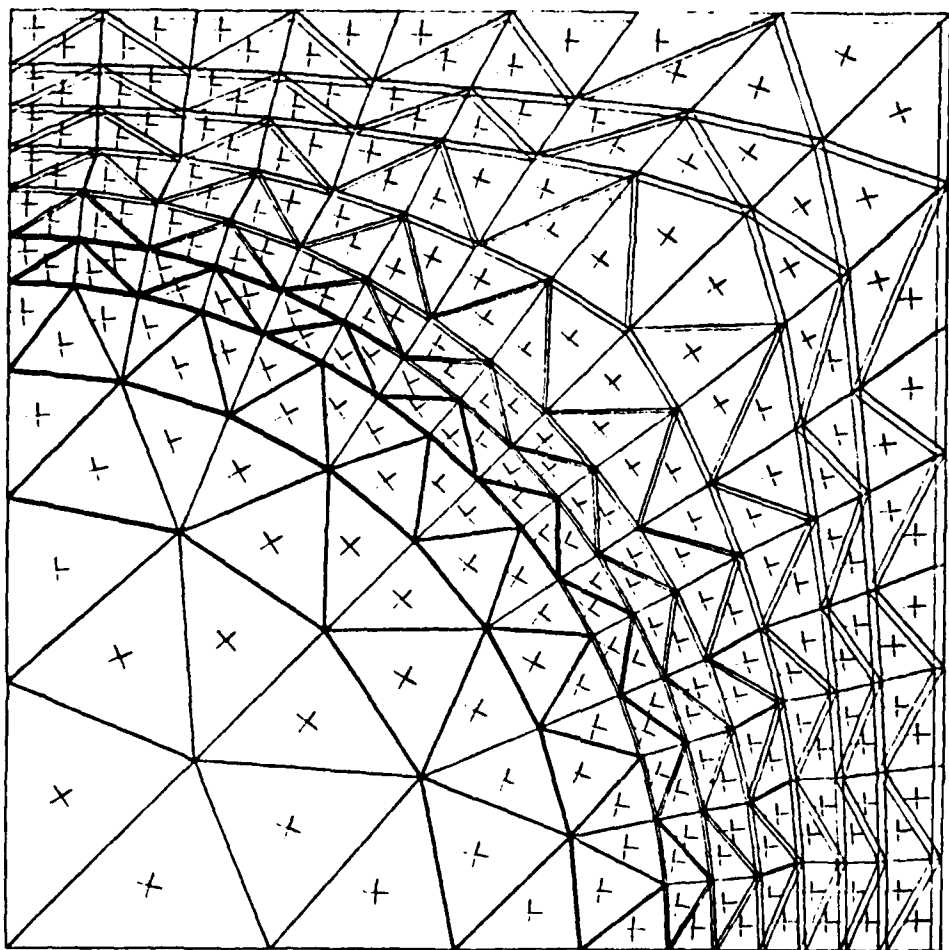


Figure 35 1% Biaxial tensile strain, large fibre,
medium plasticity interface.

Stresses in element 1 are: 143 M Pa and 143 M Pa.

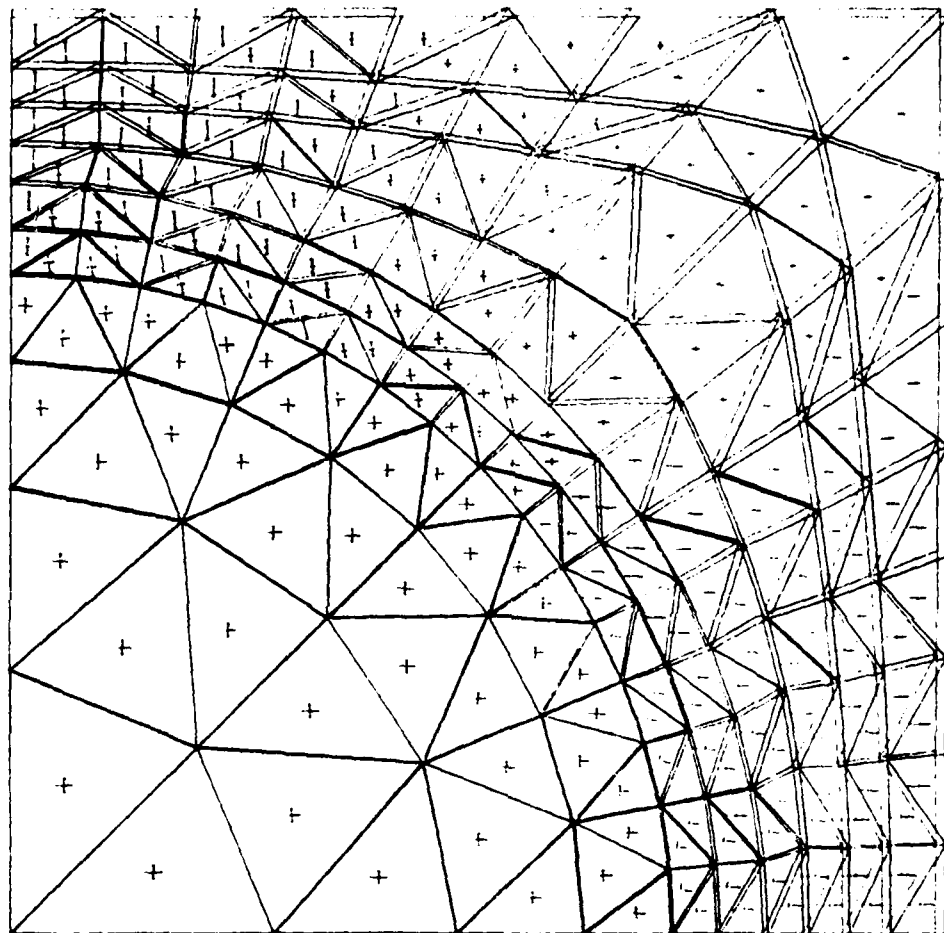


Figure 36 1% Pure shear strain, small fibre,
low plasticity interface.

Stresses in element 1 are: 47.7 M Pa and -37.4 M Pa.
Vectors with bars denote compressive stresses.

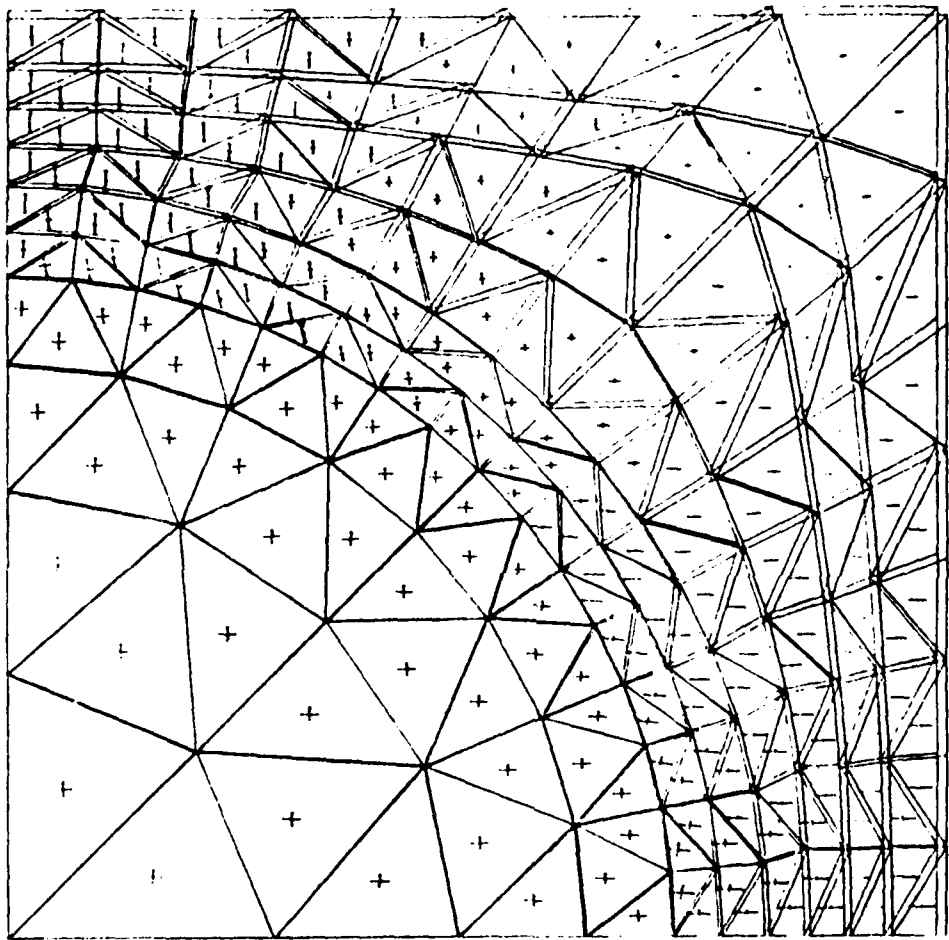


Figure 37 1% Pure shear strain, small fibre,
high plasticity interface.

Stresses in element 1 are 45.6 M Pa and -36.0 M Pa.
Vectors with bars denote compressive stresses.